LASER & PHOTONICS REVIEWS

Laser Photonics Rev. 5, No. 3, 368–403 (2011) / DOI 10.1002/lpor.201000015

Abstract Erbium-doped fiber devices have been extraordinarily successful due to their broad optical gain around 1.5–1.6 µm. Er-doped fiber amplifiers enable efficient, stable amplification of high-speed, wavelength-division-multiplexed signals, thus continue to dominate as part of the backbone of longhaul telecommunications networks. At the same time, Er-doped fiber lasers see many applications in telecommunications as well as in biomedical and sensing environments. Over the last 20 years significant efforts have been made to bring these advantages to the chip level. Device integration decreases the overall size and cost and potentially allows for the combination of many functions on a single tiny chip. Besides technological issues connected to the shorter device lengths and correspondingly higher Er concentrations required for high gain, the choice of appropriate host material as well as many design issues come into play in such devices. In this contribution the important developments in the field of Er-doped integrated waveguide amplifiers and lasers are reviewed and current and future potential applications are explored. The vision of integrating such Er-doped gain devices with other, passive materials platforms, such as silicon photonics, is discussed.

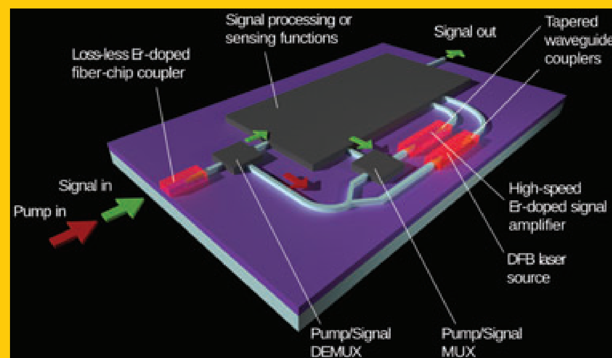

Erbium-doped integrated waveguide amplifiers and lasers

Jonathan D. B. Bradley and Markus Pollnau*

1. Introduction: Bringing the advantages of Er-doped fibers onto the chip

Since the invention of the Er-doped fiber amplifier (EDFA) in 1987 [1], it has become established as a standard component in telecom networks, facilitating information exchange worldwide. Its broad gain at important low-loss, low-dispersion wavelengths covering the telecom C- and L-bands (1525–1565 nm and 1565–1610 nm, respectively) [2, 3], low noise [4], and compatibility with fiber lightwave systems [5, 6] make it an excellent fit for signal amplification at various points in such networks. Simultaneously, the optically pumped Er-doped fiber laser (EDFL) [7] has reached a state of maturity, being ideally suited for narrow-linewidth single-frequency [8], high-power [9], multi-frequency [10–12], tunable [13–15], or short-pulse output [16–18]. EDFAs and EDFLs have been utilized in a wide range of applications, including ultra-high bit-rate telecommunications transmission systems [19], frequency measurement [20], spectroscopy [21], sensing [22], and space communications [23].

Analogous to the microelectronics industry, traditionally there has been a drive towards integrated optical devices in order to reduce the size and cost of components, particularly for the telecom world [24]. Integration allows for many components to be included in a small package and significantly reduces pump power requirements for active devices, thus improving energy efficiency. In addition to telecommunications, new applications of miniature optical devices are emerging, including, for example, on-chip optical interconnects for high-speed computing [25] and sensors via integration with other technological platforms, such as microfluidics [26, 27].

Owing to the success of the Er-doped fiber and the advantages of integrated optics in general, Er-doped waveguide devices have been intensively researched over the last 20 years [28–30]. Such devices can enhance lightwave signals or produce light at useful wavelengths, all on a robust, low-cost, miniature chip (Fig. 1). Like silica-based fibers, many materials used in integrated optics also have low losses in the 1.5 µm window, providing a motivation for utilizing amplifiers and lasers based on Er-doped waveguides in photonic circuits. The continuously decreasing size, cost, and energy requirement of diode laser pump sources has also served to improve the prospects of such devices establishing a strong market presence. A single pump source could feasibly pump many devices on the same chip.

Despite the evident advantages of Er-doped waveguide devices, integration introduces many challenges and engineering issues. Coupling light to and from miniature waveguides, efficient optical pumping, providing gain over a short length (in Er-doped fibers gain can be carried out over a meter of fiber length or more – too long for miniature chips) are but a few of the problems faced. In order to overcome these challenges, a wide range of different Er-doped waveguiding materials, integration platforms, and device designs have been studied. Early pioneering efforts in the field focused on phosphosilicate glass as a host, because of its

Integrated Optical Microsystems (IOMS), MESA+ Institute for Nanotechnology, University of Twente, P. O. Box 217, 7500 AE Enschede, The Netherlands
* Corresponding author: e-mail: m.pollnau@ewi.utwente.nl

© 2011 by WILEY-VCH Verlag GmbH & Co. KGaA, Weinheim

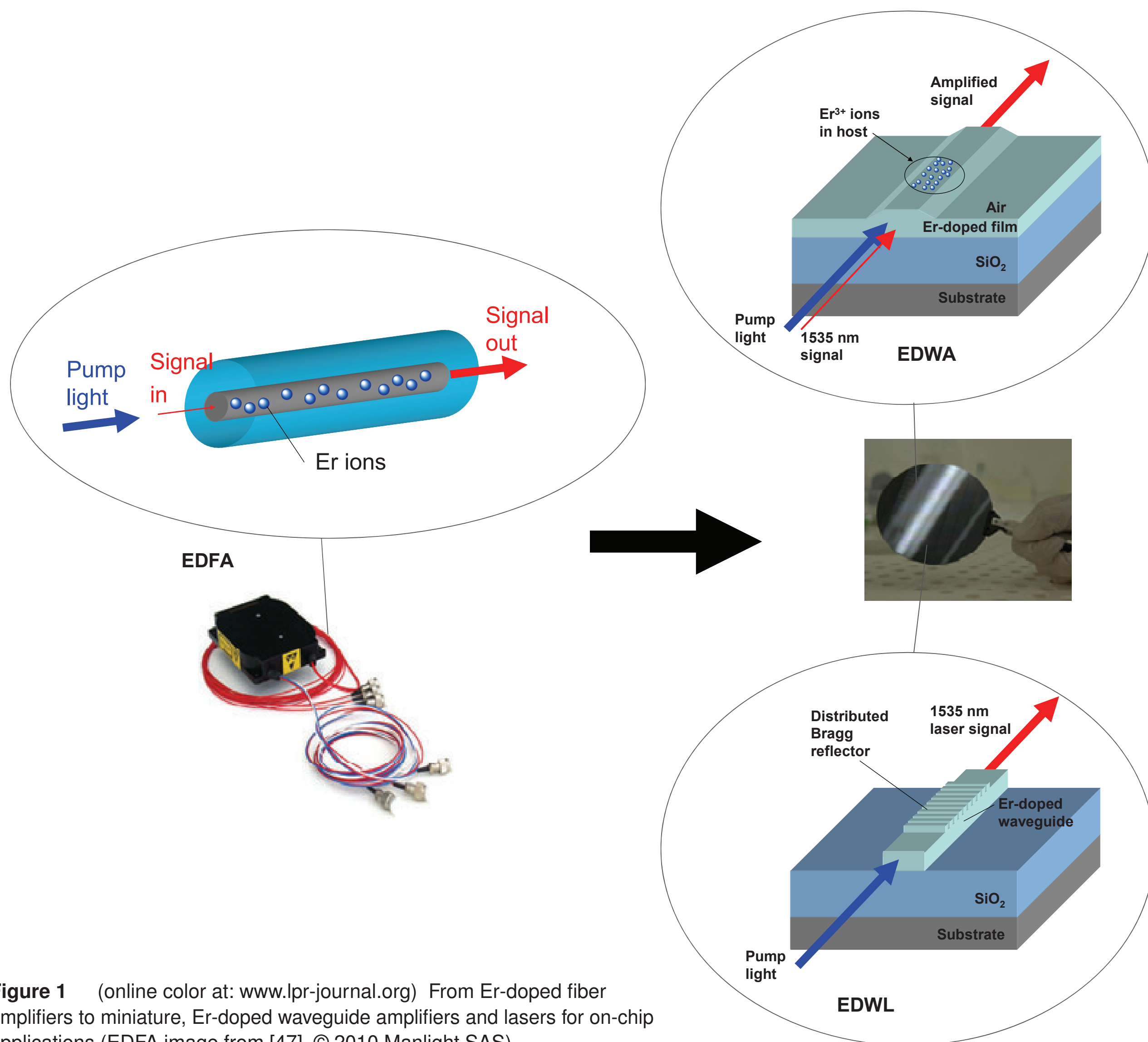

Figure 1 (online color at: www.lpr-journal.org) From Er-doped fiber amplifiers to miniature, Er-doped waveguide amplifiers and lasers for on-chip applications (EDFA image from [47], © 2010 Manlight SAS).

similarity to- and compatibility with standard silica-based optical fibers [31, 32]. At approximately the same time Er-doping of $LiNbO_3$, a common integrated optics material, was investigated, leading to amplifiers and continuous-wave and pulsed on-chip lasers [33–35]. In addition, gain was demonstrated in materials such as Al_2O_3 and Y_2O_3, where the higher refractive index contrast leads to lower pump power requirements and potentially smaller devices [36, 37]. Signal transmission experiments employing planar Er-doped glass amplifiers revealed their exceptional characteristics in telecommunications systems applications [38, 39]. The excellent properties of phosphate glass, in particular, as an Er host have been exploited, resulting in high gain amplifiers [40], high-output-power continuous-wave lasers [41] and laser arrays emitting at multiple wavelengths [42]. Much promising research has also focused on the inclusion of codopants, including Yb^{3+}-ions [43] and silicon nanocrystals [44], towards enhancing device performance via alternative pumping pathways. New directions in cavity design have led to low threshold, miniature on-chip lasers [45]. Recently, ultra-short fs-pulsed operation has been demonstrated by an on-chip Er-doped laser for the first time [44] and an ultra-narrow, 1.7-kHz-linewidth integrated Er-doped laser source has been realized [46], introducing new potential applications. Overall, these efforts have produced numerous Er-doped waveguide amplifiers (EDWAs) and lasers (EDWLs) in different materials, including crystals, glasses, and polymers. This knowledge base provides a wealth of materials and design options to select from, depending on the desired application and when considering integration with other devices and systems, be they optical, electronic, fluidic, or mechanical.

In this article we review the various approaches and the state of the art in integrated Er-doped amplifiers and lasers. We begin with an overview of the relevant Er-ion spectroscopy, followed by a survey of the wide array of Er-doped waveguiding materials and associated processing methods. EDWA and EDWL design, results and applications

© 2011 by WILEY-VCH Verlag GmbH & Co. KGaA, Weinheim

are then discussed. Finally, we examine future directions and efforts towards higher-level integration in order to provide gain and signal generation around the all-important 1.5–1.6 µm wavelength range in photonic circuits.

2. Er^{3+}-ion spectroscopy

In this section we summarize the various Er^{3+}-ion energy transitions and spectroscopic parameters most relevant to Er-doped waveguide amplifiers and lasers.

2.1. Energy levels

We first look at the relevant energy transitions in the Er^{3+} ion. The interesting optical properties of Er and other lanthanide rare earths (elements 57–71 in the periodic table) arise from the fact that they maintain an atomic-like energy structure when incorporated in a host material. Their neutral form is $(Xe)4f^{N'}5d6s^2$ or $(Xe)4f^{N'+1}6s^2$, and when incorporated in a host they are normally found in the trivalent oxidation state, whereby the weakly bound $6s^2$ electrons and either the 5d or a 4f electron are removed. The partially filled 4f electron shell is shielded by the larger-radius 5s and 5p orbitals, resulting in a localized electronic environment. Within this environment Coulomb and spin-orbit interactions lead to lifting of the degeneracy of the 4f energy levels. Thus, various distinct energy transitions within the 4f shell are possible. The seven lowest-lying energy levels of Er^{3+}, starting from the ground state and continuing up to the $^4F_{7/2}$ level are shown in Fig. 2. The levels are represented by Russell-Saunders notation $^{2S+1}L_J$, where S represents the spin angular momentum, L represents the orbital angular momentum, and J represents the total angular momentum. Each level is actually a multiplet of 2S+1 degenerate levels, which are split into S+$\frac{1}{2}$ two-fold degenerate Stark sublevels due to the crystal field imposed on the Er ion by the host matrix. Displayed in Fig. 2 are the approximate lifetimes for Er^{3+} ions in oxide glasses, energies in cm^{-1} relative to the ground state, and wavelengths corresponding to the ground-state transition from each manifold.

Several transitions relevant to Er-doped amplifiers and lasers designed for wavelengths around 1.5–1.6 µm are also shown in Fig. 2. Such devices operate based on stimulated emission on the $^4I_{13/2} \rightarrow {}^4I_{15/2}$ transition. In order to increase the population density of Er^{3+} ions excited to the $^4I_{13/2}$ level pump light at a wavelength of either ∼ 980 nm or ∼ 1480 nm is typically used. Transition (1) shows ground state absorption (GSA) of 980 nm pump light on the $^4I_{15/2} \rightarrow {}^4I_{11/2}$ transition. In oxide host materials with their rather high phonon energies this excitation is followed by rapid non-radiative decay by multiphonon relaxation to the $^4I_{13/2}$ level. Transition (2) illustrates GSA of 1480 nm pump light directly into the $^4I_{13/2}$ level. Signal light at ∼ 1530 nm can undergo GSA (3) or induce stimulated emission (4) on the $^4I_{15/2} \leftrightarrow {}^4I_{13/2}$ transition. Stimulated emission of 980 nm and 1480 nm pump light is also possible from the $^4I_{11/2}$ and $^4I_{13/2}$ levels, respectively, but is not shown in the figure.

Aside from pumping to populate the upper amplifier or laser manifold and absorption or emission of signal light, there are several additional important processes. Transition (5) represents excited state absorption (ESA) of 980 nm pump light from the $^4I_{11/2}$ level to the $^4F_{7/2}$ level [48–50]. This is a detrimental process in terms of amplifier or laser performance, leading to increased pump absorption but simultaneously decreased pump efficiency. The sixth and seventh transitions show two energy-transfer-upconversion (ETU) processes. The first process (6) involves energy transfer between two ions in the $^4I_{13/2}$ level resulting in promotion of one ion to the $^4I_{9/2}$ state and de-excitation of the other to the ground state. This process decreases the number

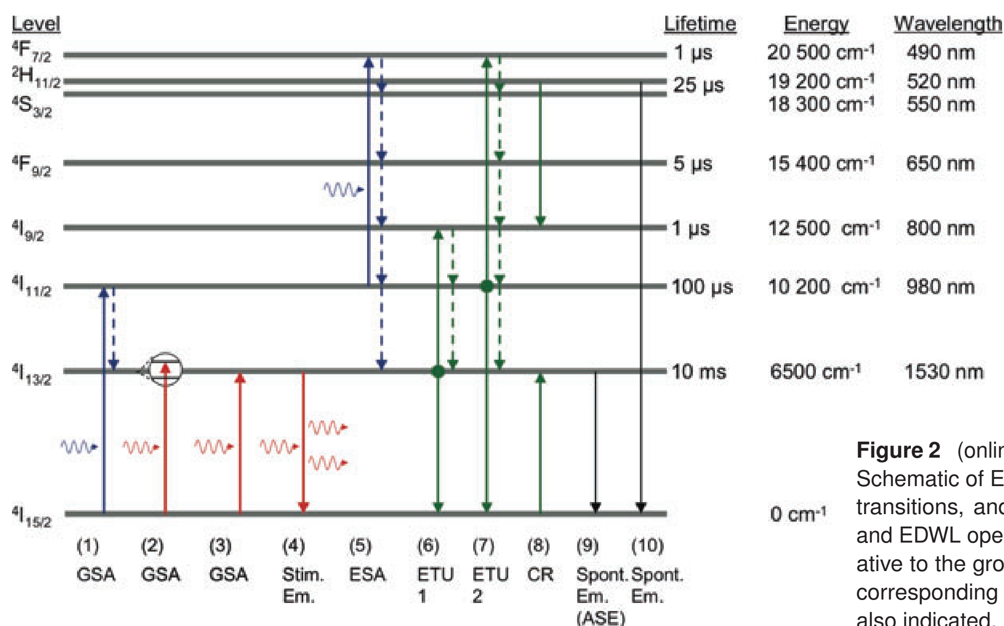

Figure 2 (online color at: www.lpr-journal.org) Schematic of Er^{3+} ion energy levels, selected transitions, and lifetimes relevant for EDWA and EDWL operation. The energy in cm^{-1} relative to the ground state and the wavelength corresponding to a photon of this energy are also indicated.

© 2011 by WILEY-VCH Verlag GmbH & Co. KGaA, Weinheim

of ions in the $^4I_{13/2}$ state available for stimulated emission, thus strongly affecting the overall gain and ultimately the amplifier or laser performance. The second ETU process (7) involves energy transfer between two ions in the $^4I_{11/2}$ state and excitation of one to the $^4F_{7/2}$ level and de-excitation of the other to the ground state. In (8) a cross-relaxation (CR) process is shown, whereby an ion in the $^4S_{3/2}$ excited state interacts with another ion in the ground state, resulting in ions exciting the $^4I_{9/2}$ and $^4I_{13/2}$ states. Finally, spontaneous emission from each manifold, governed by the decay rate (inversely proportional to the lifetime), can occur. Two important spontaneous emission processes are displayed. Transition (9) shows spontaneous emission on the $^4I_{13/2} \rightarrow ^4I_{15/2}$ transition, which releases non-coherent photons in a broad spectrum around the signal wavelength. When such light is amplified in an optical amplifier, it is referred to as amplified spontaneous emission (ASE) and it adds noise to the amplifier signal. Transition (10) represents spontaneous emission from the $^2H_{11/2}$ and $^4S_{3/2}$ levels to the ground state. It is shown, because it results in the characteristic green light visible in highly Er-doped amplifiers. A series of higher energy levels exist in Er^{3+} ions and a wide range of additional transition processes are possible, especially in host materials with lower phonon energies and accordingly longer excited-state lifetimes compared to oxides [51]. However, for the most part, those processes shown in Fig. 2 have been found to adequately describe amplifier and laser behaviour in conventional Er-doped integrated materials.

2.2. Absorption and emission cross sections

In the previous section stimulated absorption and emission of photons on various Er^{3+}-intraionic transitions were discussed. To each transition is associated a certain cross-section, which describes the probability of an excited ion emitting a photon of equal phase and frequency to a photon incident upon it (stimulated emission) or an ion being excited to a higher energy state by absorbing an incident photon (stimulated absorption). The Lambert-Beer law describes the absorption and emission of light (assuming an otherwise lossless medium) when interacting with a two-level system and over a small propagation distance Δz as follows:

$$I(z+\Delta z) = I(z)\exp\left[\sigma_{em}(\lambda)N_1(z)\Delta z - \sigma_{abs}(\lambda)N_0(z)\Delta z\right] \quad (1)$$

where $I(z+\Delta z)$ is the light intensity at distance $z+\Delta z$, $I(z)$ is the initial light intensity, $\sigma_{abs}(\lambda)$ and $\sigma_{em}(\lambda)$ are the absorption and emission cross sections (in units of cm^2) at a given wavelength λ, respectively, and $N_0(z)$ and $N_1(z)$ are the population densities of the lower and upper manifolds (density of ions in each state, in units of ions/cm^3) from which absorption or emission occurs, respectively. From this equation we obtain a stimulated absorption or emission rate per unit volume, $R_{Stim}(z+\Delta z)$, as follows:

$$R_{Stim}(z+\Delta z) = \frac{1}{E(\lambda)\Delta z}\Delta I = \frac{1}{E(\lambda)\Delta z} \times \{I(z)\exp[\sigma_{em}(\lambda)N_1(z)\Delta z - \sigma_{abs}(\lambda)N_0(z)\Delta z] - I(z)\} \quad (2)$$

where ΔI is the change in light intensity over distance Δz and $E(\lambda)$ is the energy per photon.

The absorption and emission spectra of an Er-doped material contain a set of peaks corresponding to the energies of the various intra-ionic electronic transitions. Each individual peak experiences both homogeneous and inhomogeneous broadening, which are related to the lifetime (the shorter the lifetime, the broader the energetic width of the state) and the variation in local Er^{3+}-ion environments, respectively. While in crystalline host materials the absorption and emission spectra are highly structured, the second effect is particularly strong in amorphous hosts due to the multitude of environments available, resulting in significant overlap of the peaks associated with each crystal-field transition and broad absorption and emission spectra. The absorption and emission spectra associated with each transition, while exhibiting similar peak values, are also non-identical, with absorption and luminescence being more pronounced at the short and long wavelength side, respectively, due to the Boltzmann distribution of population within each crystal-field multiplet. The theory of McCumber [52] has lead to a simple and straightforward procedure for determining the absorption spectrum in Er-doped waveguides from the emission spectrum, or vice-versa [53].

The peak values of the Er absorption and emission cross sections are typically on the order of 10^{-21}–10^{-20} cm^2, depending on the host material. The $^4I_{15/2} \leftrightarrow ^4I_{13/2}$ cross sections are of key importance in Er-doped devices operating near 1.5 µm, because they determine the probability of stimulated emission and absorption at the signal wavelength. Various peak $^4I_{15/2} \leftrightarrow ^4I_{13/2}$ cross section values are compared for both amorphous and crystalline Er hosts in Table 1. The Er cross-sections in various silicate hosts, typically used in fibers, and those of several common EDWA and EDWL host materials are included.

2.3. Lifetime

The lifetime of a given energy level is the time constant describing the exponential decay of ions from that level. It is inversely proportional to the probability per unit time of the intrinsic decay of an ion from that level. In the absence of energy-transfer processes, the luminescence decay is represented by a single exponential curve with its associated lifetime. The inverse luminescent lifetime can be written as a sum of inverse lifetimes which represent the different decay paths. These can be divided into radiative and non-radiative decay. Radiative decay results in the spontaneous emission of a photon, while non-radiative decay results in the transfer

© 2011 by WILEY-VCH Verlag GmbH & Co. KGaA, Weinheim

Host	Type	λ_{peak} [nm]	σ_{abs} [10^{-21} cm^2]	σ_{em} [10^{-21} cm^2]	Ref.
Al-P co-doped silica	Amorphous	1531	6.60	5.70	[54]
Silicate glass	Amorphous	1536	5.80	7.27	[54]
Fluorophosphate glass	Amorphous	1533	6.99	7.16	[54]
GeO_2-SiO_2	Amorphous	1530	7.9 ± 0.3	6.7 ± 0.3	[55]
Al_2O_3-SiO_2	Amorphous	1530	7.9 ± 0.3	7.9 ± 0.3	[55]
Phosphate glass	Amorphous	1535	5.4		[40]
Al_2O_3	Amorphous	1532	5.7 ± 0.7	5.7	[56]
Y_2O_3	Polycrystalline	1536	5.5	5.5	[57]
$LiNbO_3$	Monocrystalline	1534.6	24.4	24.4	[58]
Y_2O_3	Monocrystalline	1535.5	18	18	[59]
$(Gd, Lu)_2O_3$	Monocrystalline	1535.5	18	18	[59]

Table 1 Peak Er $^4I_{15/2} \leftrightarrow {}^4I_{13/2}$ absorption and emission cross sections in different host materials.

of energy to phonons, or vibrations of the crystal or glass host material. The following equation relates the various contributions to the luminescent decay from the ith level:

$$\frac{1}{\tau_i} = \frac{1}{\tau_{\mathrm{rad},i}} + \frac{1}{\tau_{\mathrm{nr},i}}, \tag{3}$$

where τ_i is the luminescence lifetime, $\tau_{\mathrm{rad},i}$ is the radiative lifetime, and $\tau_{\mathrm{nr},i}$ is the non-radiative lifetime. From this we also obtain a spontaneous decay rate, competing with stimulated emission and reducing the population density of the $^4I_{13/2}$ upper amplifier or laser manifold. The rate is simply given as $R_{\mathrm{Spont}} = N_1/\tau_1$.

Non-radiative decay occurs by energy transfer to the host material through the generation of a number of phonons with total energy equal to the energy gap between the levels, called multiphonon relaxation. The probability of multiphonon relaxation decreases exponentially with the number of phonons required to bridge the energy gap. In an ionic host, the average phonon energy is determined by the strengths of the bonds between the ions (i.e. Si^{4+} and O^{2-} in SiO_2) and the mass of the ligand anions (i.e. O^{2-}, F^-, Cl^- etc.). A lighter ligand ion and larger restoring force result in larger phonon energies. In many oxides the effective phonon energies are relatively high (900–1400 cm^{-1}), which means that the number of phonons required to bridge the gap from one level to the next is lower. Therefore, the probability of multiphonon relaxation is higher and the lifetimes of the Er excited states are usually short ($\sim$ 1–100 µs). The exception is the lifetime of the $^4I_{13/2}$ level, which remains long, because even in a high-phonon oxide host a large number of phonons is required to bridge the gap to the $^4I_{15/2}$ level. Because of the long lifetime of this level it is possible to build up population inversion, which is necessary for gain in Er-doped amplifiers. The lower phonon energies present in fluoride glasses and crystals means the $^4I_{11/2}$ energy level typically has a longer lifetime. This diminishes fast relaxation and efficient excitation of the $^4I_{13/2}$ amplifier or laser level, but favors the $^4I_{11/2} \rightarrow {}^4I_{13/2}$ laser transition at 3 µm [60, 61]; also cascade lasing of both the 3 µm and 1.5 µm transitions has been demonstrated [62–65]. The effective phonon energy and typical lifetime of the $^4I_{13/2}$ level measured in selected Er-doped host materials are shown in Table 2.

Table 2 Effective phonon energy and $^4I_{13/2}$ luminescent lifetime measured in different host materials [66–68].

Host	Type	Phonon Energy [cm^{-1}]	τ_1, $^4I_{13/2}$ [ms]
Phosphate glass	Amorphous	1200	10.7
Silicate glass	Amorphous	1100	14.7
Tellurite glass	Amorphous	700	4
Fluoride glass	Amorphous	500	10.3
Y_2O_3	Polycrystalline	400	7.2

2.4. Energy transfer between ions

Besides the intrinsic transitions between energy levels in an individual ion due to absorption, stimulated emission, and radiative and non-radiative decay, transitions caused by energy transfer between neighbouring ions play an important role. These processes, which in their most common form of electric dipole-dipole interaction exhibit a $1/r^6_{Er-Er}$ dependence on the distance between individual interacting ions, are especially important in EDWAs and EDWLs, where owing to the shorter device length and accordingly higher doping level the average inter-ionic spacing r_{Er-Er} becomes drastically smaller compared to fiber devices. Two processes involving energy transfer between ions are illustrated in Fig. 3. Figure 3a shows the process of energy migration, whereby an excited ion (the donor) transfers its energy to a nearby ion (the acceptor) in its ground state. The donor returns to the ground state while the acceptor is excited to the same state as previously occupied by the donor. This process can eventually result in loss of excitation through multiple energy-migration steps (diffusion) and ultimately quenching at an impurity such as an OH^- group. Alternatively, Fig. 3b illustrates the interaction of two excited ions, with energy from the donor being transferred to the acceptor, promoting it to a higher energy state (ETU).

© 2011 by WILEY-VCH Verlag GmbH & Co. KGaA, Weinheim

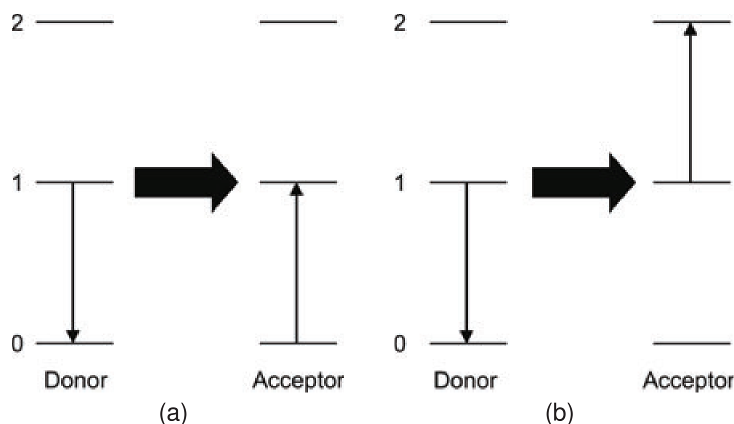

Figure 3 Er^{3+}-Er^{3+} interionic energy-transfer processes: (a) energy migration and (b) energy transfer upconversion.

In EDWAs, the ETU process from the $^4I_{13/2}$ level has a significant impact on amplifier performance, because it results in de-population of the $^4I_{13/2}$ level and re-population of the $^4I_{15/2}$ level, reducing the inversion, thus the maximum gain that can be achieved. In addition, it can lead to significant extra heat dissipation owing to the subsequent multiphonon relaxations $^4I_{9/2} \rightarrow {}^4I_{11/2} \rightarrow {}^4I_{13/2}$ of the upconverted ion [69]. In the most straightforward model, the upconversion rate is determined by a macroscopic material-dependent parameter W_{ETU} and is proportional to the square of the population density of the Er level from which it occurs [14, 15]. The upconversion rate can be represented as follows:

$$R_{\mathrm{ETU}} = W_{\mathrm{ETU}} N^2, \quad (4)$$

where R_{ETU} is the ETU rate per unit volume in ($cm^{-3}s^{-1}$), and N is the population density. The value of W_{ETU} is Er-concentration dependent and varies from host material to host material, depending primarily on the nearest-neighbor interionic spacing and the oscillator strengths and spectral overlap of the two transitions involved. Typical values of the ETU coefficient measured in Er-doped glasses originating from the $^4I_{13/2}$ level are summarized in Table 3.

The ETU strength also depends on the homogeneity of the Er^{3+}-ion distribution in the host material, which can depend on the fabrication process. For example, in [70], thin films were found to exhibit an ETU coefficient ~ 2.4 times higher than in bulk glasses. The ETU coefficients for silica-based optical fibers reported in [71] and [72] are significantly higher than- and similar to those measured in the bulk and waveguide samples, respectively. However, lower Er concentrations are typically required in Er-doped fibers, thus even for high W_{ETU} the rate and effect of ETU are relatively small. The low ETU coefficients measured in Er-doped phosphate glass and soda-lime silicate glass waveguides, even at high Er concentrations, indicates homogenous incorporation of Er^{3+} ions in those materials. This is one of the primary reasons for the high gain per unit length reported in phosphate glass and soda-lime silicate glass amplifiers. Table 3 also shows two different W_{ETU} values for Er-doped Al_2O_3 waveguides that were prepared using different fabrication methods. In amorphous Al_2O_3 thin films which were annealed after Er ion implantation the ETU parameter was determined by luminescence decay measurements to be $4 \pm 1 \times 10^{-18}$ cm^3s^{-1} for an Er concentration of 1.2×10^{20} cm^{-3} [73]. Similar films which were Er doped directly during reactive co-sputtering yielded ETU parameters on the order of 3–9×10^{-19} cm^3s^{-1} for Er concentrations of 1.2–3.6×10^{20} cm^{-3} in the same type of luminescence decay measurement [74], suggesting that a lower amount of clustering was present in these films. Nevertheless, a significant amount of non-saturable absorption was detected [74], which was interpreted as a hint towards fast quenching of a fraction of Er ions, potentially as a result of energy transfer to impurities or host matrix imperfections – or fast ETU between nearest-neighbor Er ions. A simplified amplifier model which did not take this fast-quenching effect into account resulted in higher ETU parameters [75], similar to that obtained in [73]. However, considering this effect leads to good agreement of the ETU parameters derived from luminescence decay measurements and amplifier performance and a more accurate model of amplifier behaviour [74]. Therefore, in addition to the macroscopic parameter W_{ETU}, it is important to take into account such rapid Er-impurity, Er-defect or Er-Er energy transfer processes when predicting amplifier or laser behaviour.

2.5. Gain

The fundamental process required in active Er-doped waveguide devices is optical gain. To achieve gain, the photon generation rate must be greater than the rate of photon absorption and losses to due other mechanisms, including scattering. In order to achieve gain, a pump process is required to populate the higher level from which stimulated emission occurs. This pumping can be provided by electrical means (as with semiconductor optical amplifiers) or by optical means (as with rare-earth-doped amplifiers). In the case of Er-doped materials optical pumping at a wavelength of either 980 nm or 1480 nm is typically used to excite ions from the ground state to the $^4I_{13/2}$ state (in the case of 980 nm pumping via subsequent multiphonon relaxation), from which stimulated emission can occur to amplify a signal within a rather large gain bandwidth around 1530 nm. A population inversion is required between the $^4I_{13/2}$ and $^4I_{15/2}$ state - at least 50% of ions excited to the higher energy level in case the absorption and emission cross sections are similar, i.e., at the zero-phonon line near 1530 nm. In addition, the number of stimulated emitted photons must exceed

© 2011 by WILEY-VCH Verlag GmbH & Co. KGaA, Weinheim

Table 3 ETU coefficient for the $^4I_{13/2}$ level measured in various Er-doped glasses.

Host material	Host type	Er concentration $[10^{20}\,cm^{-3}]$	ETU coefficient, W_{ETU} $[10^{-18}\,cm^3s^{-1}]$	Ref.
Aluminosilicate glass	Bulk	0.4 to 4.8	0.3 to 1.4	[70]
a-Al_2O_3	Waveguide	~ 1.2	4 ± 1	[73]
	Waveguide	1.17 to 3.66	0.29 to 0.92	[74]
Al- and Al-La-doped silica glass	Fiber	0.04 to 0.86	0.9 to 3.2	[72]
Ge/Al/P-doped silica glass	Fiber	~ 0.006 to 0.067 (70 to 840 ppm by weight)	~ 100	[71]
Phosphate glass	Bulk	1	0.77 ± 0.07	[76]
	Waveguide	1	0.93 ± 0.07	[76]
	Bulk	2.0	1.2	[77]
	Waveguide	0.2 to 4.0	~ 0.8 to ~ 1.1	[78]
	Waveguide	5.3	2.0 ± 0.5	[40]
Soda-lime silicate glass	Waveguide	~ 1.4	3.2 ± 0.8	[79]
	Bulk	0.50 to 6.0	0.26 to 1.2	[70]
	Waveguide	0.70 to 4.1	0.61 to 2.3	[70]
Fluorozirconate glass	Bulk	2; 8; 14	13; 28; 67	[80]

those lost by background losses, for example propagation losses due to scattering in a channel waveguide.

The various transition rates can be used to generate rate equations for the change of population densities of the different Er levels. These rate equations can be solved analytically, as was done using a simplified 3-level model for $Al_2O_3:Er^{3+}$ in [75] to determine the theoretical gain and performance of EDWAs and EDWLs. The magnitude of the typical waveguide cross-sections, corresponding optical intensities, and absorption and emission cross sections dictate that Er concentrations within an order of magnitude of $1 \times 10^{20}\,cm^{-3}$ (equivalent to 0.1 atomic % in amorphous Al_2O_3) are required in Er-doped waveguide devices. At higher concentrations, the close ion spacing means that gain quenching effects such as ETU begin to dominate. These parameters lead to peak gain coefficients of ~ 1–10 dB/cm in EDWAs, which means that device lengths of typically 1 cm or longer are required. For this reason it is critical to obtain low ($\ll 1$ dB/cm) background losses (the sum of scattering losses, material absorption, and all other propagation losses not related to Er^{3+}-ion absorption) for sufficiently high gain in an EDWA or EDWL.

In the literature, several different terms are frequently used to describe the gain in Er-doped waveguides. In order to properly compare the gain in different devices, it is important to distinguish between these terms. Relative gain (or signal enhancement) refers to the change in output signal with and without pump light and does not account for any losses in the waveguide, i.e., even a significant relative gain does not indicate that the waveguide losses have been compensated and signal light has been amplified. Internal net gain (or on-chip gain) represents the total amplification from the start to the end of the waveguide, i.e. internal waveguide losses are overcompensated and signal light is amplified, whereas net gain refers to the fiber-chip-fiber gain and additionally accounts for any fiber-chip coupling losses, i.e., signal light is amplified from fiber to fiber.

2.6. Er^{3+} sensitization methods

In order to enhance the Er pump rate and provide higher gain per unit length, different methods have been studied, which provide alternative excitation pathways. In particular, two methods have shown considerable promise: co-doping with Yb^{3+} ions and incorporating silicon nanocrystals in Er-doped silica waveguides. Here we examine each of these approaches.

2.6.1. Yb^{3+} co-doping

For the chosen Er concentrations of a few $10^{20}\,cm^{-3}$ pump absorption by Er ions is rather weak due to the small absorption cross sections at 1480 nm and especially 980 nm, hence device lengths of typically a few cm are used. At present, in order to achieve higher gain over shorter device lengths, Er-doped waveguide devices are customarily co-doped with Yb^{3+} ions [81, 82]. Yb^{3+}, another rare earth ion, provides an optical absorption path on the transition between its $^2F_{7/2} \rightarrow {}^2F_{5/2}$ energy levels, also centered at a wavelength near 980 nm. When Yb^{3+} ions are incorporated with Er^{3+} ions in the same host, an excited Yb^{3+} ion can transfer its energy to a neighbouring Er ion. This process is illustrated in Fig. 4: in step (i) the 980 nm photon is absorbed, which is followed by (ii) energy transfer via excitation of an Er ion to the $^4I_{11/2}$ level, and (iii) rapid non-radiative decay to the $^4I_{13/2}$ level, thus populating the upper amplifier/laser level. Step (iv) shows stimulated emission at the signal wavelength. While back-transfer to the Yb^{3+}

© 2011 by WILEY-VCH Verlag GmbH & Co. KGaA, Weinheim

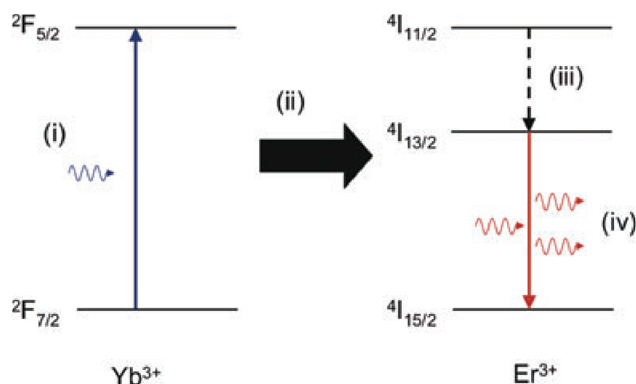

Figure 4 (online color at: www.lpr-journal.org) Primary processes involved in Er^{3+} sensitization by Yb^{3+} co-doping: (i) 980 nm pump light absorption and excitation of Yb^{3+} ion; (ii) energy transfer from an excited Yb^{3+} ion to an Er^{3+} ion in the ground state; (iii) fast non-radiative decay of an excited Er^{3+} ion from the $^4I_{11/2}$ level to the $^4I_{13/2}$ level; (iv) stimulated emission at 1.5 µm.

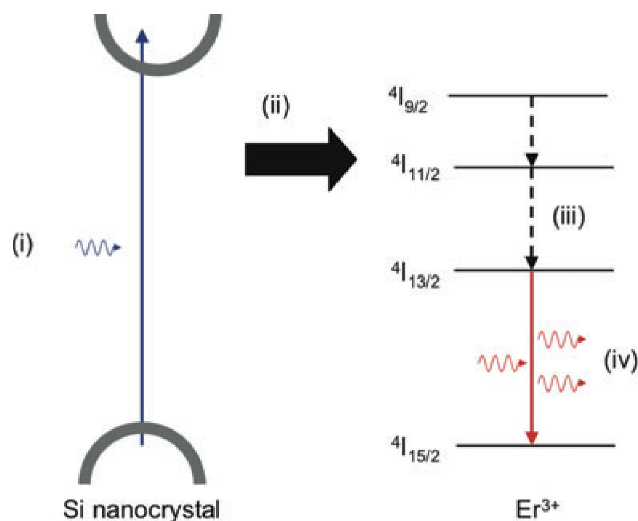

Figure 5 (online color at: www.lpr-journal.org) Er sensitization by resonant energy transfer from Si nanocrystals: (i) electron-hole pair excitation by short-wavelength pump light in Si-nc; (ii) energy transfer from Si-nc to Er ion; (iii) fast non-radiative decay of an excited Er^{3+} ion from the $^4I_{9/2}$ level to the $^4I_{13/2}$ level; (iv) luminescence or stimulated emission at 1.5 µm.

ion may occur, rapid decay of the excited Er^{3+} ion by multi-phonon relaxation to the $^4I_{13/2}$ level is more likely, making this an effective excitation process.

Since it does not introduce reabsorption at the signal wavelength around 1530 nm, the Yb^{3+} ion with its similar radius and ionic properties can be incorporated in concentrations comparable to or higher than Er^{3+}. Besides, the $Yb^{3+2}F_{7/2} \rightarrow {}^2F_{5/2}$ absorption cross-section can be almost an order of magnitude higher than the Er^{3+} pump absorption cross section around 980 nm [56]. When suitable Er and Yb concentrations are selected and the pump power is sufficiently high, the additional Er-excitation pathway provided by the Yb^{3+} ions increases the overall pump rate, effectively competing with de-excitation due to ETU. Therefore, a key advantage of Yb co-doping is that it can help overcome Er-ion concentration quenching effects, allowing for higher Er concentrations and potentially higher gain per unit length.

2.6.2. Si nanocrystals

Another sensitization method, which continues to be intensively researched due to its promise of providing a completely silicon-compatible amplifier or laser, is by co-doping Er-doped silica with Si nanocrystals (Si-nc's) [83–85]. The Si-nc's, from 1 to 10's of nm in diameter, absorb light over a broad wavelength range and, when coupled with Er, can efficiently transfer energy to Er ions. This process is illustrated in Fig. 5.

The main potential advantage of sensitization by Si-nc's is an effective Er excitation cross-section that is orders of magnitude higher than the Er absorption cross section [86]. A higher effective excitation cross-section arises because the probability of photo-excitation of the numerous charge carriers in a Si-nc, followed by subsequent energy transfer to a nearby Er^{3+} ion, is much higher than that of direct Er^{3+} ion excitation via photon absorption on the various parity-forbidden intra-4f transitions. In addition, Si-nc's have a broad absorption band in the UV-visible range, where low-cost diode lasers and LEDs are available as pump sources. Another advantage for silica, in particular, is the effective refractive index enhancement of the material by Si-nc doping, resulting in better optical confinement [87].

However, specific obstacles continue to hamper this method of sensitization. Auger non-radiative electron-hole pair de-excitation reduces the excitation density [88]. In addition, signal photon absorption by confined excited carriers within the Si-nc's competes with the signal enhancement [89]. Furthermore, resonant energy transfer from Si-nc's, which often exhibit peak photoluminescence intensities at around 800 nm, to Er can result in an excited state transition from the $^4I_{13/2}$ to the $^4S_{3/2}$and $^2H_{11/2}$ manifolds, thus decreasing the overall excitation efficiency [90]. The full energy-transfer model is still the subject of great debate [91–94], and perhaps with future optimization of the Er concentration, nanocrystal size and distribution [95] the promise of more efficient amplifiers and lasers via Si-nc sensitization will be realized.

3. Materials for Er-doped integrated optical devices

A key consideration in the design and realization of Er-doped devices is the choice of host material. Many Er-host materials have been investigated for integrated optical applications. In this section the requirements of the host material are discussed and amorphous and crystalline hosts are compared. A summary of the numerous methods that have been applied to fabricate Er-doped waveguides is also given.

© 2011 by WILEY-VCH Verlag GmbH & Co. KGaA, Weinheim

3.1. Er^{3+}-ion host material requirements

Much of the research on EDWAs and EDWLs has focused on studying various planar waveguide host materials. There are several requirements which must be met in order for a material to be considered a suitable Er host. These include properties relating to the incorporation of Er in the host and those related to integrated optical devices in general. Requirements relating to Er doping are summarized below.

1. *Suitable Er^{3+}-ion bonding sites*. The host material must possess appropriate bonding sites for the trivalent Er ion. For crystalline materials, the sites must be non-centro-symmetric, in order for mixing of opposite parity wavefunctions of the 4f states to occur, making the various electric-dipole forbidden transitions within the 4f orbital possible. In addition, the size of the lattice position must be sufficiently large for the Er^{3+} ion (ionic radius ≈ 103 pm). For example, Er-ion incorporation is prevented in α-Al_2O_3 (the crystalline form of Al_2O_3, or sapphire) due to an ionic radii mismatch. However, Er can be incorporated in high concentrations in a-Al_2O_3 (amorphous Al_2O_3) because of the presence of a range of suitably sized bonding sites. The oxide of Er is Er_2O_3, so sesquioxides, such as Y_2O_3, Sc_2O_3, Lu_2O_3, with similar cationic radii, tend to be excellent hosts.
2. *High Er solubility without clustering.* In comparison to fiber devices, a high Er solubility is essential for shorter Er-doped waveguide devices. For reasonable gain in Er-doped waveguide devices, concentrations of 1 to 10 × 10^{20} ions/cm^3 (0.1 to 1 atomic %) are typically needed. The nearest Er-ion distance depends on the host material and the doping method. In order to reduce quenching due to ETU, clusters of Er^{3+} ions should be avoided.
3. *A long $^4I_{13/2}$ radiative lifetime.* A long (∼ ms) $^4I_{13/2}$ radiative lifetime is required in order to provide sufficient population buildup for gain at reasonable pump rates.
4. *Low phonon energy*. The host should have a low effective phonon energy to prevent gain quenching through non-radiative decay.
5. *High purity.* Defects and impurities in the host material should be avoided in order to prevent lifetime quenching through non-radiative decay.

In addition to those properties pertaining to Er doping, the host should possess several general properties motivating its application in integrated optical devices. These properties are discussed below.

1. *Optically isotropic.* For applications requiring complex integrated designs, the host material should have the same refractive index in all directions.
2. *Good physical and chemical properties.* The host must have sufficient hardness and mechanical stability, as well as being chemically stable. In order to avoid over-heating and damage at high optical pump powers it should also have high thermal stability and thermal conductivity.
3. *Fabrication technology.* The ability to deposit or grow thin films or substrates of sufficient size at a reasonable cost and using a straightforward doping mechanism is required. The technology must also be compatible with the intended device specifications and application. For example, the possibility to grow Er-doped layers on a specific substrate may be desirable. Furthermore, a method for defining channel waveguides in the host material is required. Some hosts, although providing excellent physical properties, including chemical stability, are difficult to structure for this very reason [96].
4. *Low background losses.* The waveguiding material should have low background optical propagation losses at pump and signal wavelengths. Sources of loss in films or substrates include the intrinsic absorption of the material and scattering or absorption at impurities and the interface between layers. In addition, the method used to define channel waveguides should not significantly increase the losses (for example, by scattering of the propagating light at rough channel waveguide sidewalls).

3.2. Amorphous vs. crystalline hosts

Er host materials can be broadly divided into two categories: crystalline (or poly-crystalline) and amorphous hosts. This natural division arises from the significant difference in the spectroscopic characteristics of Er in each type of material. Each type of material has potential advantages, depending on the required application.

Crystalline and polycrystalline materials offer sharp emission lines, high peak cross sections, and high stability for narrow-band amplifier and laser applications. As shown in Table 4, crystalline materials can be further divided into dielectric [34, 68, 97–100] and semiconductor hosts [101, 102]. Dielectric crystalline materials have a large band gap, thus are highly transparent over a wide wavelength range. However, by definition, they do not permit efficient electrical excitation, limiting their use to all-optical applications. In semiconductor hosts, electro-optic properties can be exploited, allowing integration of Er-doped devices with electro-optic and electrical devices. The high refractive index contrast in such materials also allows for high integration density. However, due to the lack of suitable Er^{3+}-ion bonding sites, it is generally difficult to achieve practical Er concentrations in semiconductors. While Er incorporation in III-V semiconductors has been investigated [101], such materials are already excellent light emitters. In addition, Er incorporation in silicon, which is a poor light emitter because of its indirect bandgap, has been studied extensively with the aim of developing a monolithic silicon light source. Electrically pumped light emitting diodes have been demonstrated [103, 104]. However, only limited success has been realized due to ionic radii mismatch, resulting in low Er^{3+}-ion solubility, and the presence of strong non-radiative recombination pathways [105]. Since Er incorporation in silicon is limited, significant research efforts have instead focused on Er-doped silica containing Si nano-clusters, with encouraging results [106]. The main drawbacks of crystalline materials in general are the narrow gain spectrum, limiting their usefulness for amplifiers or on-chip tunable lasers, and the fact that they can only be grown on lattice-matched substrates, hence cannot be easily integrated with other materials platforms.

© 2011 by WILEY-VCH Verlag GmbH & Co. KGaA, Weinheim

Table 4 Integrated optics host materials for Er

Host Type	Category	Examples	Advantages	Disadvantages
Amorphous	Glass	a-Al_2O_3 Bismuthate glass Fluoride glass Phosphate glass Silicate glass	Broad emission spectrum; high stability; deposition on a variety of substrates; optically isotropic	Low refractive index contrast
	Polymer	6-fluorinated-dianhydride/epoxy PMMA PPMA	Broad emission spectrum; low cost; deposition on a variety of substrates	Thermal instability; colour centers
Crystalline	Dielectric	$(Gd, Lu)_2O_3$ $KY(WO_4)_2$ $LiNbO_3$ $Y_3Al_5O_{12}$ $YAlO_3$ Y_2O_3	High emission and absorption cross sections; highly stable output (lasers); high thermal conductivity	Narrow wavelength range (for amplifiers or tunable lasers); epitaxial growth on specific substrates required
	Semiconductor	GaAs GaN InP Si ZnO	High emission and absorption cross sections; monolithic integration of integrated optical and electro-optic devices; High integration density	Narrow wavelength range; epitaxial growth required; low Er solubility

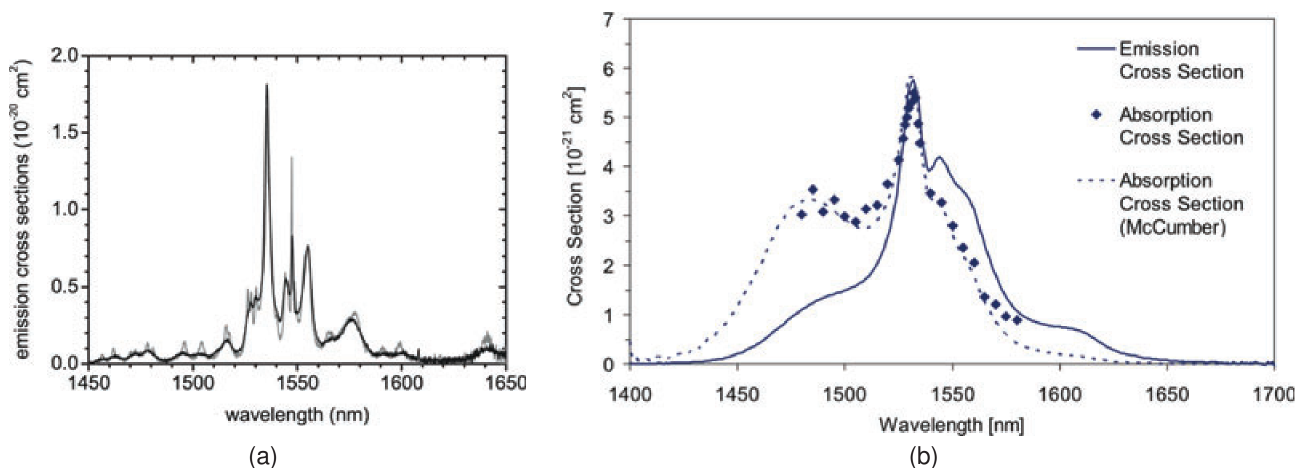

Figure 6 Er $^4I_{13/2} \rightarrow ^4I_{15/2}$ emission cross section measured in Er-doped (a) crystalline $(Gd, Lu)_2O_3$ film (black curve) and a Y_2O_3 bulk crystal (gray curve) (from [59], © 2008 Optical Society of America) and (b) an Er-doped amorphous Al_2O_3 thin film (absorption cross section also shown) (from [75], © 2010 Optical Society of America).

In contrast to crystalline materials, amorphous hosts exhibit broad emission spectra due to both homogenous and inhomogenous broadening. The lack of periodicity in amorphous materials results in a multitude of local Er environments and the superposition of each of these transition spectra creates an overall broadened transition linewidth for the Er ion. While the peak emission cross-sections are lower as compared to crystalline hosts, the broad smooth emission spectrum affords relatively flat gain over a wide wavelength range, an advantage exploited in EDFAs and tunable Er-doped lasers. Emission spectra for crystalline and amorphous Er-doped host materials are compared in Figs. 6a and b, respectively. Amorphous hosts can also be sub-divided into two groups of materials: polymers and glasses (see Table 4). Polymer waveguides are of interest due to their low cost and straight-forward integration with other materials and have shown promise as rare-earth hosts [107–113]. However, the thermal stability of such materials is poor and the host material itself often exhibits additional absorption lines (colour centers). Amorphous Er-doped glasses exhibit a broad emission spectrum, generally possess a high thermal stability, and can be deposited on a wide range of substrates. Because of these advantages, and the success of Er-doped glass fiber amplifiers and lasers,

© 2011 by WILEY-VCH Verlag GmbH & Co. KGaA, Weinheim

many glass host materials have been investigated for active planar devices. These include silicate glass [32, 114–117], phosphate glass [39, 81, 118–124], fluoride glass [125], and amorphous aluminum oxide [36, 126–129]. In addition, multi-component oxide glasses [38, 130–145] offer the possibility to tailor various properties such as the gain spectrum and the refractive index. Glass hosts have relatively low refractive indices, which are closely matched to those of standard optical fibers. This index-matching is a distinct advantage for low-loss coupling to optical fibers. However, the lower index is a disadvantage compared to semiconductor devices in terms of achieving large integration density. Nevertheless, their high Er solubility, broad gain, and low cost makes them highly useful for integrated active devices. The remaining sections of this review focus primarily on glass and dielectric hosts because of their excellent properties for broadband amplifier and tunable laser applications and the significant research effort which has been aimed at developing EDWAs and EDWLs in these materials.

3.3. Waveguide fabrication methods

Numerous fabrication methods have been studied for Er-doped active devices, each with different advantages and disadvantages, depending on the desired application. There are several possibilities when selecting the fabrication procedure. The first consideration is the growth of the Er-doped host material. The host material can be grown in the form of a substrate, for example, from a glass melt. In contrast it may be deposited or grown on an existing substrate using one of several standard deposition technologies. Another consideration is the doping method. The Er dopant may be incorporated into the film/substrate during growth or added after via ion implantation or other techniques. Finally, channel waveguides with suitable dimensions and low losses must be defined. Waveguides are patterned using a variety of techniques, including physical etching by reactive ion etching, ion beam etching or, more recently, direct writing using a femtosecond pulsed laser. The applicability of the technique depends on the host material itself.

Er-doped and Er-, Yb-co-doped substrate and thin film growth techniques are summarized in Table 5. Growth methods can be divided into substrate growth vs. layer deposition. Substrate growth methods include Czochralski crystal growth [99] and melting of appropriate precursors followed by cooling [125, 130, 144, 146, 147], as is employed to fabricate commercial Er-doped silicate and phosphate glasses [118, 119, 148–150]. The advantage of entire substrate growth is the high purity and excellent control over the uniformity and concentration of doping. A drawback of such methods is the difficulty in combining such materials with other integrated optics platforms. In contrast, thin film growth methods typically involve deposition on oxidized silicon wafers (the oxide layer on the silicon providing the lower cladding layer) or other substrates, thus potentially allowing for integration with other devices on the same substrate and fabrication of devices over a large area. Methods which have been utilized for depositing Er-doped waveguiding films include atomic layer deposition [129, 151], dip-coating [152], flame hydrolysis [32, 153], high vacuum chemical vapour deposition (HV-CVD) [154], plasma-enhanced chemical vapour deposition (PECVD) [83, 127, 138, 155–157], pulsed laser deposition (PLD) [59, 126, 145, 158–163], reactive co-sputtering [68, 84, 87, 128, 164–166], RF-sputtering [40, 98, 131, 133, 137, 167–170], the sol-gel method [134, 171–183], spin coating [108, 109], and vapour phase deposition [125, 184].

In addition to those techniques mentioned, an important consideration is the doping method. Most of the techniques discussed involve doping of the host during growth or deposition, resulting in a uniform Er-ion distribution throughout the medium. However, the Er profile and separation can be controlled by using alternating targets. This has been investigated for Er-doped and Er-, Yb-co-doped alumina thin films using PLD [185–188]. One of the advantages of this technique is that the Er concentration can be tailored such that it is highest where the pump light intensity is highest, thus potentially improving the pumping efficiency. Another advantage is the ability to control the Er-Er ion separation in one dimension, potentially reducing Er-Er ion interactions and gain quenching through ETU. Alternatively, Er can also be introduced after host material production by ion implantation [36, 79, 85, 86, 189–193] or indiffusion [34]. Besides allowing for control of the dopant profile, both methods provide the added advantage of selectively doping certain areas of the chip, thus providing gain only where it is needed. This can eliminate losses related to Er absorption in sections of the chip designed for passive devices. The drawbacks of such techniques, especially ion implantation, are the additional cost and processing steps required. Specifically, this includes the equipment costs associated with the operation of an ion implanter and post-implantation, high-temperature annealing. Our research group utilizes reactive-co-sputtering to deposit Er-doped Al_2O_3 films [164]. This technique introduces Er during film growth and yields as-grown active layers which are uniform, are of high optical quality, and have low optical propagation losses (~ 0.1 dB/cm at 1320 nm).

After the Er-doped film or substrate is prepared, channel waveguides must be defined in order to guide the light on chip. Several different methods which have been applied to define Er-doped channel waveguides are summarized in Table 6. The waveguide fabrication techniques can be conveniently divided into those that modify the local physical properties and refractive index of the layer or substrate and those that change the geometry of the layer. In direct-writing techniques such as femtosecond laser writing [147, 179, 194–196] and focused proton beam writing [197], the local refractive index in the bulk material is modified at a specific point and the substrate is scanned to write the waveguide. The refractive index modification occurs at the focal point of the high-energy pulses and in the ion-implanted region for femtosecond laser writing and focused proton beam writing, respectively. He^+ ion implantation [99], ion exchange [118, 119, 123, 125, 130, 136, 144, 146, 148, 149, 198–200], and ion indiffusion [34, 81] are also used to alter the local refractive index through photolithography and

© 2011 by WILEY-VCH Verlag GmbH & Co. KGaA, Weinheim

Table 5 Er-doped and Er, Yb co-doped host material fabrication methods for integrated optics

Er-doped host material fabrication method	Host materials	References
Atomic layer deposition	a-Al_2O_3	[129]
	Y_2O_3	[151]
Czochralski crystal growth	$YAlO_3$	[99]
Dip-coating	ZnO nanoparticle colloid	[152]
Er-indiffusion	$LiNbO_3$	[34]
Er ion implantation	a-Al_2O_3	[36]
	AlGaAs	[189]
	Amorphous silicon	[190]
	Silicon	[191]
	Si-nc/SiO_2	[85, 86, 193]
	Soda-lime silicate glass	[79]
	Y_2O_3	[192]
Flame hydrolysis	Phosphosilicate glass	[32, 153]
HV-CVD	a-Al_2O_3	[154]
Melting/cooling	Borosilicate glass	[130, 146]
	Fluoride glass	[125]
	Lanthanum sodium silicate glass	[150]
	Phosphate glass	[118, 119, 148, 149]
	Phosphotellurite glass	[147]
	Soda-lime aluminosilicate glass	[144]
PECVD	Aluminogermanosilicate	[138]
	a-Al_2O_3	[127, 155]
	Phosphosilicate glass	[156]
	Si-nc/SiO_2	[83, 157]
Pulsed laser deposition	a-Al_2O_3	[126]
	$(Gd, Lu)_2O_3$	[59]
	Oxyfluoride silicate glass	[145]
	Phosphate glass	[158]
	YAG	[159]
	Y_2O_3	[160–162]
	ZnO	[163]
Reactive co-sputtering	a-Al_2O_3	[128, 164]
	Silicon nitride	[165]
	Si-nc/SiO_2	[84, 87]
	Y_2O_3	[68]
	Zirconia	[166]
RF-sputtering	Aluminosilicate glass	[137, 167, 168]
	a-Al_2O_3	[169]
	Bismuthate glass	[170]
	Phosphate glass	[40]
	Sodium-calcium silicate glass	[131]
	Soda-lime silicate	[133]
	YAG	[98]
Sol gel method	Aluminophosphosilicate glass	[175, 177]
	Aluminosilicate glass	[171]
	a-Al_2O_3	[172]
	GeO_2-based glass	[134]
	Germano- and alumino-phosphosilicate	[176]
	glass	[178, 179]
	Oxyfluoride silicate glass	[180]
	Silica	[173, 174]
	Silica-titania	[181]
	TiO_2	[182]
	$Y_2Ti_2O_7$	[183]
	Y_2O_3	
Spin-coating	Polymer	[108, 109]
Vapour phase deposition	Fluoride glass	[125]
	Silicon monoxide	[184]

© 2011 by WILEY-VCH Verlag GmbH & Co. KGaA, Weinheim

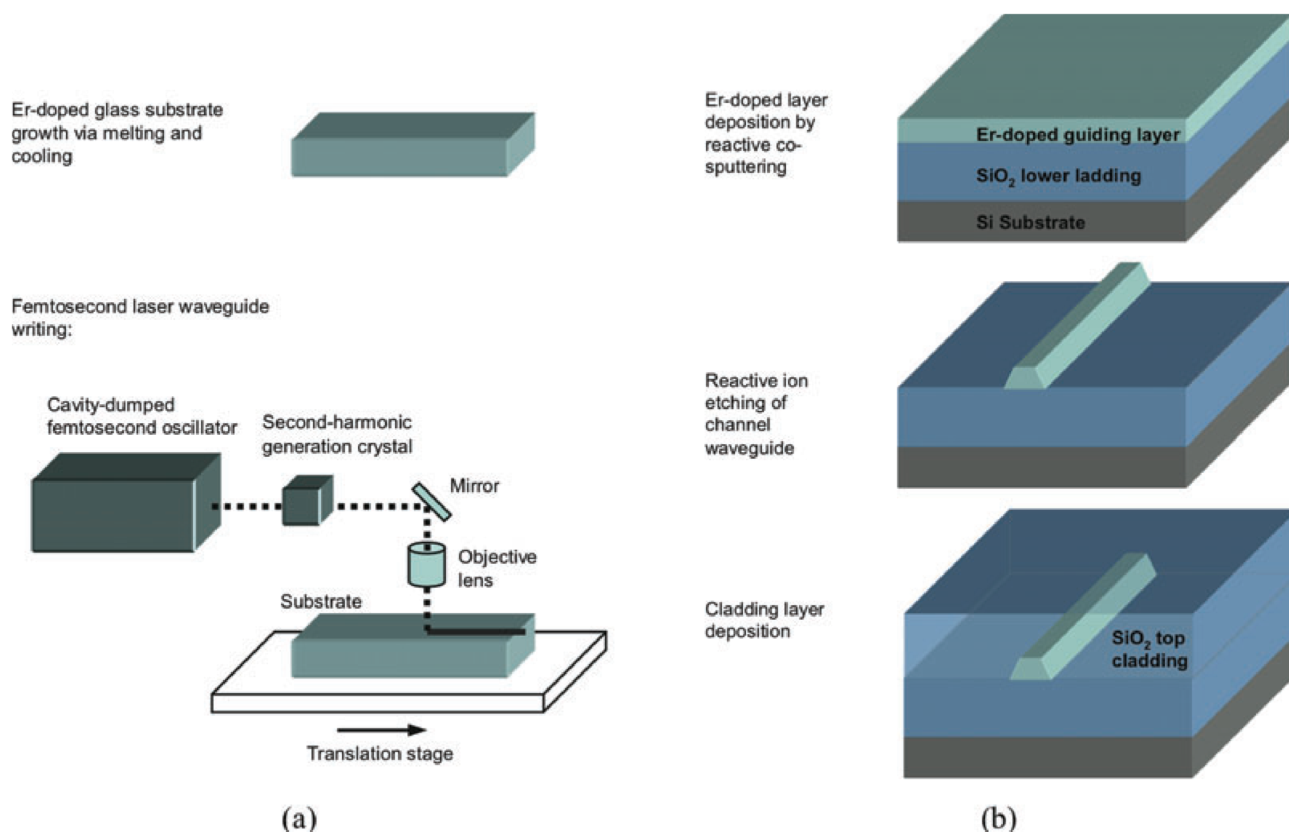

Figure 7 (online color at: www.lpr-journal.org) Er-doped waveguide fabrication methods: (a) femtosecond laser writing directly into an Er-doped glass substrate (adapted from [204]); (b) Er-doped layer deposition followed by reactive ion etching and passivation by top-cladding deposition.

patterning over a large wafer area. Typically, the index change which results from these methods is on the order of 1×10^{-3} to 1×10^{-2}. Therefore, they are useful for defining relatively large cross-section glass waveguides, similar to the ~ 9-µm core width found in single-mode optical fibers designed for 1550 nm. Lateral confinement can also be achieved in planar waveguiding films by etching rib or ridge waveguide structures. Etching techniques include Ar-ion beam etching [36, 68, 128, 131, 133, 201], etching either the substrate [123, 125] or over-layer (strip-loading) [40, 87, 150, 174], reactive ion etching (RIE) [32, 59, 75, 108, 109, 137, 138, 145, 153, 156, 169, 170, 175, 176, 193], and wet chemical etching [79, 129, 152, 157, 166, 177]. Of these etching methods, RIE provides the best control and resolution. However due to the excellent mechanical and chemical stability of certain Er-doped hosts, such as Y_2O_3, such dry chemical etching can be difficult due to the lack of a suitable etch chemistry [96]. For these materials physical sputtering via Ar-ion beam etching must be utilized. In general, the aim of any etching method should be smooth sidewalls in order to prevent high scattering losses. Using femtosecond laser writing, ion exchange, or etching methods background losses (losses besides those due to Er absorption) on the order of ~ 0.1 dB/cm or less can be achieved in Er-doped glass channel waveguides [199, 202, 203].

Two differing approaches to Er-doped waveguide fabrication are compared in Fig. 7. In Fig. 7a, glass substrate formation from a glass melt followed by femtosecond laser writing is shown. This method is serial, thus greatly increasing the time and cost for patterning over large areas or multiple substrates. However, a key advantage is its inherent flexibility to define waveguides at different depths in the substrate, allowing for three-dimensional photonic circuits to be written. In Fig. 7b, Er-doped waveguide deposition by reactive co-sputtering, followed by reactive ion etching and top cladding deposition is shown. We use this approach to fabricate $Al_2O_3:Er^{3+}$ active devices on standard thermally oxidized silicon wafers. This and similar methods allow for large-area wafer-scale processing using standard micro-fabrication equipment. The parallel nature of waveguide writing is preferable when large-batch processing is required. In summary, a number of approaches to Er-doped waveguide device fabrication have been established. The various techniques allow for flexibility when designing photonic systems using EDWAs and EDWLs.

4. Er-doped waveguide amplifiers

In this section EDWA design, performance, and potential applications are explored. Various approaches to amplifier design and layout are discussed. The gain characteristics of different Er-doped waveguiding materials and applications in telecom and other novel areas are also reviewed.

© 2011 by WILEY-VCH Verlag GmbH & Co. KGaA, Weinheim

Table 6 Techniques utilized for fabrication of Er-doped channel waveguides

Channel waveguide fabrication method	Host materials	References
Ar-ion beam etching	Al_2O_3	[36, 128]
	Phosphate glass	[201]
	Sodium-calcium silicate glass	[131]
	Soda-lime silicate	[133]
	Y_2O_3	[68]
Femtosecond laser writing	Bismuthate glass	[196]
	Oxy-fluoride silicate glass	[179, 194]
	Phosphate glass	[195]
	Phosphotellurite glass	[147]
Focused proton beam writing	Phosphate glass	[197]
H^+ or He^+ ion implantation	$YAlO_3$	[99]
Ion exchange	Borosilicate glass	[130, 146]
	Fluoride glass	[125]
	Germano-silicate glass	[136]
	Phosphate glass	[118, 119, 123, 148, 149, 198–200]
	Soda-lime aluminosilicate glass	[144]
Ion indiffusion	$LiNbO_3$	[34]
	Phosphate glass	[81]
Lithography and substrate etching	Fluoride glass	[125]
Reactive ion etching	Aluminogermanosilicate glass	[138]
	Aluminophosphosilicate glass	[175]
	Aluminosilicate glass	[137]
	Al_2O_3	[75, 169]
	Bismuthate glass	[170]
	$(Gd, Lu)_2O_3$	[59]
	Germano- and alumino-phosphosilicate	[176]
	glass	[145]
	Oxyfluoride silicate glass	[32, 153, 156]
	Phosphosilicate glass	[108, 109]
	Polymer	[193]
	Si-nc/SiO_2	
Strip-loading	Phosphate glass	[40]
	Lanthanum sodim silicate glass	[150]
	Silica-titania	[174]
	Si-nc/SiO_2	[87]
Wet chemical etching	Aluminophosphosilicate glass	[177]
	Al_2O_3	[129]
	Si-nc/SiO_2	[157]
	Soda-lime silicate glass	[79]
	ZnO nanoparticle colloid	[152]
	Zirconia	[166]

4.1. Amplifier design

Significant research has focused on EDWA design, with the goal of optimizing gain and achieving maximum efficiency in short devices. Here we examine the various aspects of EDWA design and the different approaches to each aspect.

4.1.1. Gain optimization

Several parameters are involved in the design of EDWAs, each affecting the gain response and pump power requirements of the amplifier. Here we divide those parameters into material and design parameters, although the latter are also influenced by the material. The main parameters affecting amplifier performance are summarized in Table 7.

The absorption and emission cross sections, fluorescent lifetime, ETU coefficient, and background loss are all determined by the Er-doped host material. The absorption and emission cross sections, including the ESA cross section, and bandwidth of the absorption/emission spectra depend on the local Er environment. Therefore, the peak cross-section values and spectral bandwidth vary for the different glass hosts most commonly used for EDWAs. The $^4I_{13/2}$ fluorescent lifetime is typically on the order of ~ 10 ms, although

© 2011 by WILEY-VCH Verlag GmbH & Co. KGaA, Weinheim

Table 7 Parameters affecting gain in Er-doped waveguides.

Type	Parameter
Material	Absorption and emission cross sections
	Fluorescent lifetime
	ETU coefficient
	Background loss
Design	Waveguide cross section
	Amplifier length
	Pump wavelength
	Signal wavelength
	Pump power
	Signal power
	Er concentration

it and the shorter lifetimes of the higher energy levels vary depending on the effective phonon energy of the host. The $^4I_{13/2}$ lifetime also depends on the fabrication method, as impurities can lead to lifetime quenching. The ETU coefficient is both Er-concentration and host-material dependent and can largely affect amplifier performance. In Er-, Yb-co-doped amplifiers, $Er^{3+} \leftrightarrow Yb^{3+}$ energy transfer coefficients also play a role. With suitable fabrication methods background losses of typically 0.1 dB/cm or less can be achieved in most glass host materials.

The parameters selected by the EDWA designer include the geometrical waveguide cross section, amplifier length, pump wavelength, and Er concentration. The waveguide cross section depends on the refractive index contrast of the waveguide core and cladding materials. In silica waveguides, for example, the relatively low contrast results in waveguide cross-sections similar to optical fibers ($> 10\,\mu m^2$). A smaller waveguide cross section generally allows for a smaller mode-field diameter. This increases the intensity incident on each Er ion, thus enhancing the rate of stimulated absorption or emission. Higher refractive index materials such as Al_2O_3 permit smaller waveguide cross-sections ($< 5\,\mu m^2$), thus higher intensities and lower pump-power requirements. The selected waveguide cross section and refractive index contrast also determine the confinement of light within the waveguide core. Pump or signal light which propagates in the cladding of the waveguide does not interact with Er ions and is not absorbed or amplified, respectively, thus a higher confinement is desired. The amplifier length must be chosen to provide sufficient excitation of Er ions throughout its entire length, based on the available pump power. Excessive pump absorption in the beginning could lead to low excitation at the end of the waveguide and re-absorption of amplified signal light. The gain depends on the pump wavelength, typically 980 nm or 1480 nm, as will be discussed in the next sub-section. It also depends on the signal wavelength because the Er absorption and emission cross sections are wavelength-dependent. The Er energy level population dynamics depend on the pump and signal powers, which determine the rate of interactions with Er ions in their various states. Therefore the gain strongly depends on the pump and signal powers launched into the device. Finally, the Er concentration determines the maximum gain that can be achieved.

It becomes clear that once a given material is optimized, the various design parameters largely determine the response of the amplifier, including the maximum gain. EDWA and Yb-co-doped EDWA performance has been investigated theoretically in a number of hosts [43,58,75,205–210]. Such theoretical simulations are applied, for example, to select the optimum input pump power and wavelength, waveguide cross section and length, and Er concentration for a given input signal power and wavelength. In most cases excellent agreement with the experimental response was obtained, providing a valuable tool for designing EDWAs.

4.1.2. Pumping Schemes

One of the key engineering issues with Er-doped waveguide amplifiers is the coupling of pump and signal light to and from the chip. Traditionally the $\geqslant 100$ mW of 980 nm or 1480 nm pump light, provided from a III-V diode or other laser, is launched into the end of the chip from an optical fiber. The reduced cost of diode laser pump sources begins to make commercial packaged Er-doped waveguide devices more practical. In addition, their stable operation without temperature controllers reduces the size and power demands, allowing for overall compact devices (see for example [211]). Efficient fiber-chip coupling can be achieved using traditional end-polishing and precision alignment methods, and a single pump source could be used to excite simultaneously several devices.

The method chosen for pumping depends on the demands of the application. Multiplexing and de-multiplexing of pump and signal light can occur off chip or on-chip. Off-chip (de-)multiplexing can be facilitated using a standardized WDM fiber coupler. Such an approach is appropriate for an EDWA operating in place of an EDFA in a fiber-lightwave system. However, to pump several devices, or for on-chip applications it is desirable to couple/decouple pump and signal light in an integrated manner. On-chip 980/1530 nm [114] (see Fig. 8a) and 1480/1530 nm [36] multiplexers have been demonstrated using wavelength-dependent directional couplers. A segmented asymmetric y-junction can also be applied [212]. In addition to pumping in one direction, bi-directional pumping is also often utilized in order to excite Er ions from both ends of the waveguide [195]. Such a pumping scheme can be especially beneficial when the active waveguide has a high Er concentration and the pump light tends to be absorbed over a short length.

In addition to end-coupling of both, pump and signal, or coupling over a relatively short distance on-chip via directional couplers, gradual pump-coupling schemes have been proposed. In such a scheme the pump light is introduced into the waveguide progressively along its length, resulting in more uniform Er excitation and gain throughout the waveguide. Closely spaced waveguides [213] or hybrid photonic

© 2011 by WILEY-VCH Verlag GmbH & Co. KGaA, Weinheim

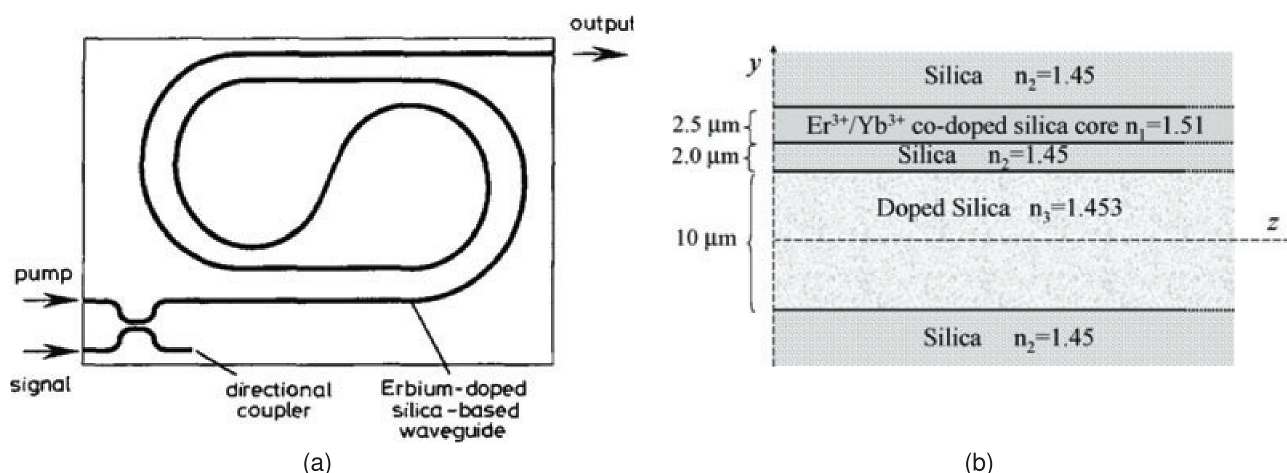

Figure 8 On-chip pump coupling schemes: (a) integrated 980/1530 nm directional coupler (from [114], © 1994 IEE) and (b) distributed multimode waveguide coupler (from [215], © 2007 IEEE).

crystal waveguides [214] have been proposed to achieve excitation in this manner. A longitudinal multimode pumping scheme has also been investigated theoretically [215–218] (see Fig. 8b). Such a method could provide more efficient pump-chip coupling via broad area lasers. Another pump method altogether is using top-mounted LEDs to excite the waveguide. In [106], an array of low-cost GaN LEDs were used to excite a Si-nanocrystal sensitized Er-doped silica waveguide over a length of 5 mm. By butt-coupling such an LED array to the waveguide, power densities of up to 20 W/cm^2 can be achieved.

The most efficient wavelengths for pumping EDFAs and EDWAs are 980 nm and 1480 nm. In specific situations 980 nm pumping results in higher maximum population inversion, hence higher gain at the signal wavelengths around 1530 nm [61]. This is because the $^4I_{13/2}$ level with its long lifetime has a large population density. As a consequence, stimulated emission at 1480 nm from the upper Stark levels of the $^4I_{13/2}$ manifold and the $^4I_{15/2}$ ground state becomes significant at higher excitation densities, making the active medium transparent for the pump. In contrast, under 980 nm pumping, Er^{3+} ions experience rapid non-radiative decay from the $^4I_{11/2}$ level to the $^4I_{13/2}$ level. Therefore, stimulated emission from the $^4I_{11/2}$ level is less prominent. As we have seen, 980 nm pumping is also required in the case of Er-, Yb-co-doped waveguides in order to excite the Yb^{3+} ions. While in other situations 1480 nm pumping can offer higher maximum gain, it can also ease waveguide design and improve amplifier efficiency. This is because it is much more straightforward to design waveguides which are single-mode at both 1480 nm and 1530 nm, as opposed to 980 nm and 1530 nm. It also eases fiber-chip input/output coupling in the case where pump and signal are injected/collected through a single fiber. Pumping at 1480 nm also typically reduces the threshold pump power for achieving net gain because of better overlap of pump and signal beams and the higher photon flux per unit pump intensity at this wavelength as compared to 980 nm.

980 nm and 1480 nm pumping have been compared both theoretically [219] and experimentally [75, 167]. In Fig. 9

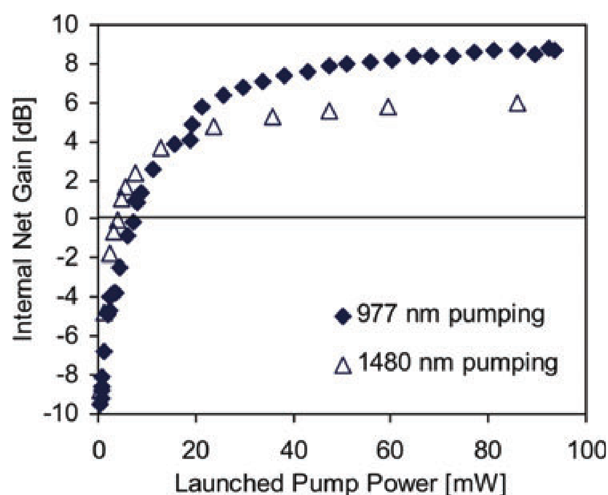

Figure 9 Gain at 1533 nm versus launched pump power for an Al_2O_3:Er^{3+} amplifier with an Er concentration of 1.17 × 10^{20} cm^{-3} and pump wavelengths of 977 nm and 1480 nm (from [75], © 2010 Optical Society of America).

the net gain at 1533 nm is compared when pumping a 5.4-cm-long Al_2O_3:Er^{3+} waveguide amplifier with a dopant concentration of 1.17 × 10^{20} cm^{-3} at each wavelength. Under 980-nm pumping, the threshold pump power for internal net gain is 7 mW, while the gain begins to saturate above 20 mW, before reaching a value of approximately 9 dB for a launched pump power of almost 100 mW. By comparison, under 1480 nm pumping, the threshold pump power is almost a factor of two lower (4 mW), while the total gain saturates at a value of only approximately 6 dB.

4.1.3. Co-doping

In addition to Er, other active co-dopants, in particular other rare-earth ions, can be of interest for integrated amplifiers. As mentioned previously, when pumping at 980 nm Yb co-doping can be advantageous. The higher pump absorption

© 2011 by WILEY-VCH Verlag GmbH & Co. KGaA, Weinheim

rate due to both, a relatively high Yb concentration and absorption cross-section combined with efficient Yb-Er energy transfer, reduces performance degradation due to Er ion-ion interactions (ETU) [43, 205]. The effect becomes particularly important as the Er concentration is increased and the ETU rate increases. By applying Yb co-doping the pumping efficiency can be increased and the device length shortened in both Er-doped waveguide amplifiers and lasers. The optimum concentrations and doping ratio have been investigated theoretically [124, 206, 207, 209, 220], resulting in typical Yb:Er concentration ratios of 1:1 to 10:1. Besides Yb, other rare-earth co-dopants, such as Tm (1460–1530 nm, 1700–2100 nm) and Pr (1300–1400 nm), can be utilized for extending or adding additional amplification bandwidth [221].

In [106], Lee et. al. demonstrated evidence of gain in a Si-nanocrystal-sensitized, Er-doped silica waveguide. They reported up to a maximum gain of 3 dB/cm (with unknown waveguide propagation losses) using 470-nm LED top-pumping, and predicted full inversion in the top-pumped region of the waveguide. Silver has also been investigated for sensitization, resulting in enhanced photoluminescence when using short pump wavelengths (360 nm and 488 nm) [222]. Another Er sensitizer which has been considered is Eu. It was found to increase the branching ratio of the $^4I_{11/2}$ level towards the $^4I_{13/2}$ state, resulting in a higher steady-state population of the upper amplifier or laser level [192]; this can be especially interesting in materials with lower effective phonon energies.

4.1.4. Device scaling

An important aim of EDWA research has been to reduce the scale of devices in order to minimize the footprint and improve the efficiency. A key parameter in terms of scaling of integrated optical devices is the refractive index difference Δn between core and cladding. Compared with semiconductors such as silicon and III-Vs, the refractive index of the waveguide core in glass materials is significantly lower, thus reducing the index difference that can be achieved. The refractive index of various dielectric Er host materials is compared in Table 8. Generally, a higher Δn allows for smaller

Table 8 Refractive index difference between core and SiO_2 cladding ($n_{Cladding} \approx 1.45$) in various Er-doped glass waveguides (all indices at a wavelength of ~1550 nm).

Host Material	Refractive Index n_{Core}	Refractive Index Difference Δn	Ref.
Phosphosilicate glass	1.46	0.01	[233]
Phosphate glass	1.55	0.10	[40]
Aluminosilicate glass	1.61	0.16	[167]
Al_2O_3	1.65	0.20	[75]
Y_2O_3 (poly-crystalline)	1.90	0.45	[57]
Bismuthate glass	1.94	0.49	[232]

Figure 10 (online color at: www.lpr-journal.org) Top view image of a 4-cm-long spiral Er-doped waveguide wrapped up to fit in a chip area of ~1x1 mm^2. Green light owing to spontaneous emission on the $^2H_{11/2}/^4S_{3/2} \rightarrow ^4I_{15/2}$ transition is visible (Reprinted with permission from [230]. Copyright 2003, American Institute of Physics.).

waveguide bend radii without resulting in severe leakage of the optical mode and high losses. However, a trade-off exists between the lower minimum bend radius and increased scattering loss at the core-cladding interface due to higher Δn. For silica-clad, phosphosilicate-core waveguides, bend radii in excess of 1 mm are required in order to minimize losses [32]. Owing to the higher index difference in Al_2O_3 waveguides, bend radii on the order of 250 µm are practical [223]. Therefore, the potential for miniature devices in combination with our recent results suggests a promising future for this material [224]. EDWA layout optimization has been investigated taking into account the waveguide geometry and bend losses, with the result being a spiral or folded approach to reducing the device footprint [225–229]. Fig. 10 shows a 4-cm-long spiral waveguide amplifier wrapped up to fit in a chip area of only 1 mm^2 [230].

In addition to the bend radius, the channel waveguide cross-section can be decreased in higher index waveguides. This increases pump intensity and signal confinement in the waveguide, decreasing the threshold pump power and improving gain efficiency. By reducing the waveguide cross-section from upwards of 10 µm^2, as is the case in silica-based fibers, to $\leqslant$ 2 µm^2, amplifiers with gain of several dB and requiring less than 10 mW of launched pump power have been demonstrated [36, 37, 40]. At the same time, in such small-core integrated amplifiers fiber-chip coupling losses tend to increase due to mode-mismatch. In large-core EDWAs with waveguide cross-sections which are well-matched to standard single-mode optical fibers the fiber-chip coupling loss can be reduced to < 0.2 dB [231]. However, efforts to reduce coupling losses in small-core EDWAs by using on-chip mode-converters resulted in minimal losses of 0.25 dB per converter and total coupling losses of only 0.65 dB per fiber-EDWA interface [167]. In order to enhance the potential for integration of EDWAs within photonic circuits, investigation of higher index glass hosts will be essential. One example of such a promising material is bismuthate glass, with a refractive index of up to 1.94 measured at the signal wavelength [232].

© 2011 by WILEY-VCH Verlag GmbH & Co. KGaA, Weinheim

Table 9 Comparison of maximum internal net gain measured in different integrated Er-doped waveguide amplifier host materials.

Host	Er conc. [10^{20} cm^{-3} or as indicated]	Yb-co-doped?	Sample length [cm]	Background loss [dB/cm]	Pump power[1] [mW]	Peak internal net gain[2] [dB/cm]	Ref.
Phosphate glass	2.3 wt%	Yes	3.1	0.4	460	5.3	[82]
Soda-lime silicate glass	4.3	No	2.4	1	120	4.2	[234]
Bismuthate glass	0.63 wt%	No	8.7	0.2	1050	2.3	[196]
Borosilicate glass	2.4	Yes	3.9	0.15	130	2.3	[132]
Al_2O_3	2.12	No	2.1	0.14	80	2.0	[75]
$LiNbO_3$	Not reported	No	5.7	0.1	170 (1484 nm)	2.0	[34]
Aluminosilicate glass	Not reported	No	5	0.2	130	1.9	[167]
Oxyfluoride silicate glass	1.1	Yes	1	0.34	342 (980 and 1480 nm)	1.9	[179]
Y_2O_3	1.3	No	4.3	0.9	10 (1480 nm)	1.3	[37]
Fluoride glass	Not reported	No	1.9	0.6	340 (1480 nm)	1.3	[125]
Aluminophospho-silicate glass	0.25 mol%	Yes	5	< 0.2	175	1.1	[139]
Polymer	1 wt%	No	1.6	< 1	70	0.84	[108]
Phosphosilicate glass	0.48 wt%	No	7.5	0.17	420	0.67	[156]
Phosphotellurite glass	0.7	No	2.5	1.35	220	0.5	[147]

[1]Pump wavelength indicated in brackets if a wavelength other than 975 to 980 nm was used.

[2]For a signal wavelength ranging from 1530 to 1540 nm or 1555 nm (phosphotellurite glass).

4.2. State of the art

As we have seen, a number of parameters are involved in the amplifier design, each of which must be carefully selected in order to achieve the highest possible gain at minimal pump power and in a minimum device footprint. Selection of the waveguide dimensions is critical to ensure a large overlap of the optical signal with the active waveguide core. The choice of pump wavelength, typically either 980 nm or 1480 nm, also affects the amplifier performance. In addition, Er-Er ion and impurity quenching effects and the channel waveguide propagation losses must be minimized. These last parameters are a strong function of the host material. Thus, in essence, the maximum gain which can be achieved is limited by the host material.

A survey of EDWAs of length 1 cm and longer and fabricated from different materials is presented in Table 9. They are compared in terms of substrate type, Er concentration, sample length, background loss, pump power, and maximum small-signal internal net gain. Among these, Er-doped phosphate, soda-lime silicate, bismuthate, borosilicate, aluminosilicate and oxyfluoride silicate glasses, Al_2O_3, and $LiNbO_3$ have emerged as excellent EDWA materials due to ease of fabrication, high Er solubility without introducing significant quenching effects and, as a result, comparatively high net gain per unit length. Peak gain of 3–5 dB/cm around 1535 nm are typically reported in Er-doped and Er-, Yb-co-doped phosphate glass [40, 82, 115, 123, 124, 198, 199] and soda-lime silicate glass [38,234] amplifiers with up to 4.1 dB total gain also demonstrated in a short, highly Er-, Yb-co-doped (8-wt.% Er^{3+} and 12-wt.% Yb^{3+}) phosphate glass amplifier of only 3-mm length [81]. Gain of 5.3 dB/cm was demonstrated at 1534 nm using bi-directional pumping, also in an Er-, Yb-co-doped phosphate glass amplifier [82]. Ultra-high dopant concentrations and Yb-co-doping bear further investigation, in particular in combination with smaller waveguide dimensions, so the pump threshold can be reduced. Pump powers in excess of 100 mW are often injected to demonstrate such high gain. However, in [36], significant steps were made towards reducing EDWA footprint and pump power requirements. A peak gain coefficient of 0.58 dB/cm was reported at 1.53 μm in a miniature 4-cm-long spiral Er-doped Al_2O_3 amplifier for a launched pump power of only 9 mW. Recently higher peak gain of 2.0 dB/cm was shown in a similar material [75]. Two different Er-doping methods were used, ion-implantation and reactive co-sputtering, and the amplifiers had different waveguide cross-sections ($0.6{\times}2$ and $0.9{\times}4$ μm^2), although each amplifier had similar dopant concentrations (2.7 and 2.12 $\times 10^{20}$ cm^{-3}). The lower ETU parameters measured in [74] for the latter fabrication method appear to be offset by other fast-quenching energy-transfer mechanisms, as discussed in Sect. 2.4. The primary differences between the two amplifiers contributing to the higher gain in the latter case were

© 2011 by WILEY-VCH Verlag GmbH & Co. KGaA, Weinheim

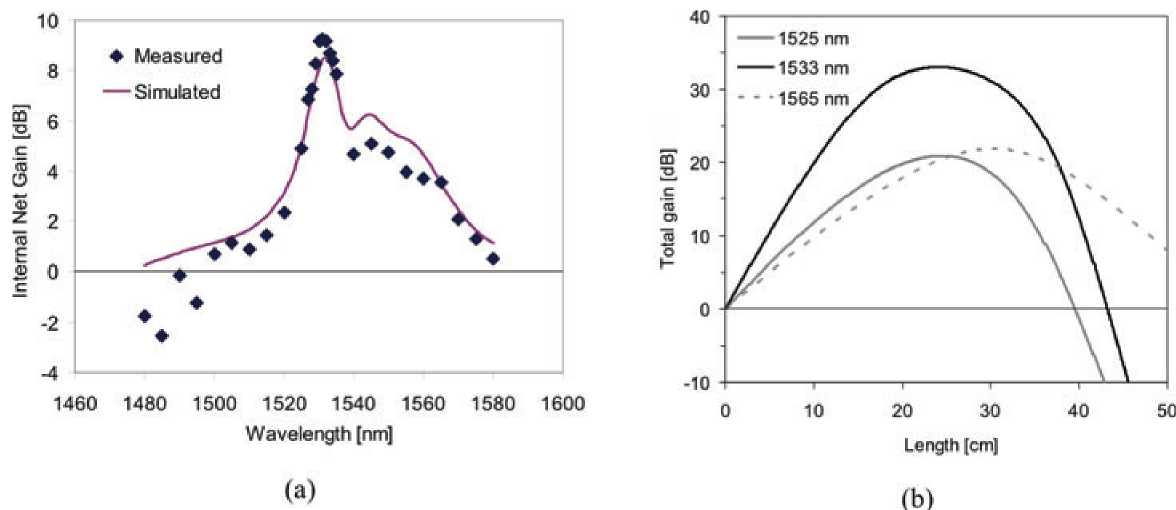

Figure 11 (online color at: www.lpr-journal.org) Broadband amplification in Al_2O_3:Er^{3+} waveguides: (a) measured and simulated internal net gain as a function of wavelength for an amplifier length of 5.4 cm, Er concentration of 1.17×10^{20} cm^{-3}, and a launched pump power of 80 mW; (b) simulated total internal net gain at 1525 nm, 1533 nm, and 1565 nm vs. waveguide length for an Er concentration of 2.0×10^{20} cm^{-3}, launched signal power of 1 μW, and launched pump power of 100 mW (from [75], © 2010 Optical Society of America).

a lower background loss (0.13 dB/cm vs. 0.35 dB/cm at the signal wavelength), a higher maximum excitation density facilitated by the choice of pump wavelength (980 nm vs. 1480 nm), and a greater optical field confinement within the Er-doped core (85% vs. 36% at the signal wavelength). In another demonstration of considerably reduced pump threshold, only 10 mW of pump power was required for 5.7 dB total gain at 1536 nm in a 4.3-cm-long Er-doped polycrystalline Y_2O_3 amplifier [37]. Furthermore, only 21 mW of pump power was required for 4.1 dB total gain at 1535 nm in the 1-cm-long Er-doped phosphate glass amplifier reported in [40]. Peak gain of $\geqslant$ 2.0 dB/cm has also been demonstrated in Er-doped bismuthate glass [196] borosilicate glass [132], and $LiNbO_3$ [34]. Other Er-doped materials exhibiting net gain include various multicomponent silicate glasses [139, 167, 179], fluoride glass [125], polymer [108], and phosphotellurite glass [147].

In addition to the peak gain, the gain bandwidth is an important property, particularly for wavelength division multiplexing applications. Materials such as Al_2O_3:Er^{3+} offer a wider emission spectrum than silica [127], and amplification has been demonstrated over an 80 nm range in Al_2O_3:Er^{3+} channel waveguides (1500–1580 nm) [75]. Figure 11a shows the measured and simulated internal net gain vs. wavelength in a 980-nm-pumped, 5.4-cm-long Al_2O_3:Er^{3+} and Fig. 11b shows the predicted gain in a longer amplifier at the gain peak (1533 nm) and at the edges of the C-band (1525 nm and 1565 nm). Net on-chip gain of $\geqslant$ 20 dB is predicted in a 24-cm-long amplifier over the C-band. Wide emission spectra have also been demonstrated in other glass hosts, including bismuthate glass [232] and phosphotellurite glass [147]. In the latter example internal gain was also demonstrated over an 80 nm range, covering the telecom C- and L-bands (1530–1610 nm). With broadband amplifier and tunable laser applications in mind, these figures are highly promising.

4.3. Applications

EDWAs provide high and broad gain on a miniature chip, allowing for compact fiber-pigtailed components for boosting the signal in an optical transmission system. Their compact size and potential for mass production make them ideal for emerging applications such as fiber-to-the-home. They also provide the potential for integration with other devices for compensation of losses or signal boosting within an integrated photonic circuit. Broad and high gain in standalone fiber-pigtailed devices (fiber-chip-fiber gain) with a view towards commercial applications and mass-production has been reported [40, 81, 82, 119, 123, 124]. In addition, a commercial EDWA, displayed in Fig. 12, has been produced, which provides 27 dB over a wavelength range of 30 nm [235]. Such a device is competitive in terms of per-

Figure 12 (online color at: www.lpr-journal.org) Image of a commercial packaged Er-doped waveguide amplifier (from [235], © 2010 Teem Photonics).

© 2011 by WILEY-VCH Verlag GmbH & Co. KGaA, Weinheim

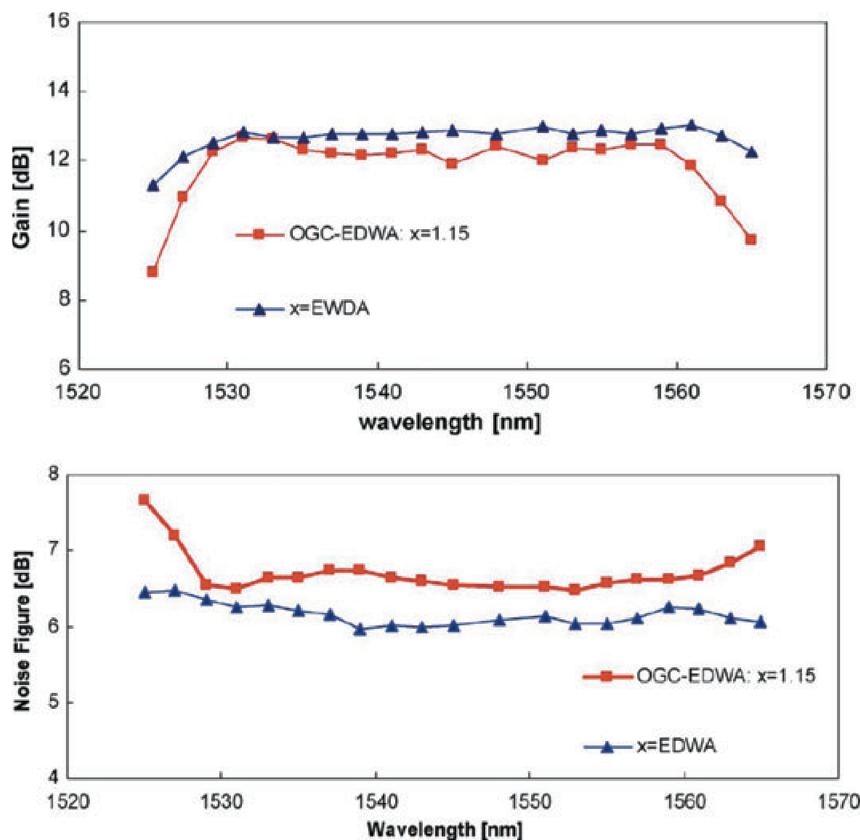

Figure 13 (online color at: www.lpr-journal.org) Gain (top) and noise figure (bottom) characteristics of a regular EDWA and an optical gain clamping (OGC) EDWA operating 15% over lasing threshold (x = 1.15) (from [238], © 2007 IEEE).

formance and cost with well-established EDFAs and semiconductor optical amplifier components [236].

Traditionally, the main motivation for EDWA technology has been its potential application in telecom systems. Like EDFAs, the long excited-state lifetime means they are insensitive to signal transients. Parameters such as the amplified spontaneous emission (ASE), noise figure, and bit error rate (BER) have been studied in systems experiments [38, 39, 167] with results competitive with widely-employed EDFAs. EDWAs have been deployed experimentally in various positions in – and in different types of – networks, including within WDM ring networks [237–239], in CATV networks [240], as a high-output-power post-amplifier [241], and in METRO networks [117, 242]. In [117, 242], signal-transient insensitive operation was demonstrated, while gain clamping was demonstrated in [243] using a feedback loop. In [238], flat gain and noise figures were demonstrated over the C-band in a regular EDWA and using in-band lasing to suppress relaxation oscillations and spectral hole burning offset (see Fig. 13 top and bottom, respectively). The compact size, low noise figure, and signal-transient insensitivity of EDWAs has also been exploited by utilizing an EDWA as a pre-amplifier in a 40 Gbit/s photoreceiver module [244]. In [245], open eye diagrams and negligible effect on the system bit error rate was demonstrated in a 170 Gbit/s transmission experiment (see Fig. 14a and b, respectively). This performance may pave the way for their future use in low-cost compact optical interconnects and high-speed photonic circuits.

Besides signal losses after propagation over long distances, certain optical functions performed in components in a fiber-lightwave system or on a chip result in an immediate reduction in signal power. One such basic function is splitting an optical signal into multiple channels. Amplification before, after, or during splitting can compensate for the 3 dB loss each time a signal divides. The short device length associated with Er-doped waveguides means compact lossless splitters are possible. Lossless 1×2 and 1×4 power splitters [132, 203, 231, 246, 247] and an amplifying 4×1 combiner [115] have been demonstrated using Er-doped waveguides. In [203], we demonstrated zero-loss power splitting for low pump power (< 50 mW) over a wavelength range of 40 nm (see Fig. 15). Commercial planar 1×4 and 1×8 power splitter modules based on EDWAs have also been developed [235].

EDWAs have been utilized in numerous other experiments, wherever signal enhancement is required using a compact device. Another useful application of EDWAs is as an amplifying element in a fiber ring laser [248–250], where such a device is practical due to its short length (see Fig. 16). EDWAs have also been investigated for amplification of laser signals for large-scale sensing applications [251]. Several applications have also been demonstrated using Er:$LiNbO_3$ waveguides. These include an acoustically tunable wavelength filter with gain [252], see Fig. 17, a spectrum analyzer with internal gain [253], and production and interference of photon echoes for demonstrating the feasibility of long-distance quantum communication [254]. In addition, pump-controlled all-optical switching in non-linear

© 2011 by WILEY-VCH Verlag GmbH & Co. KGaA, Weinheim

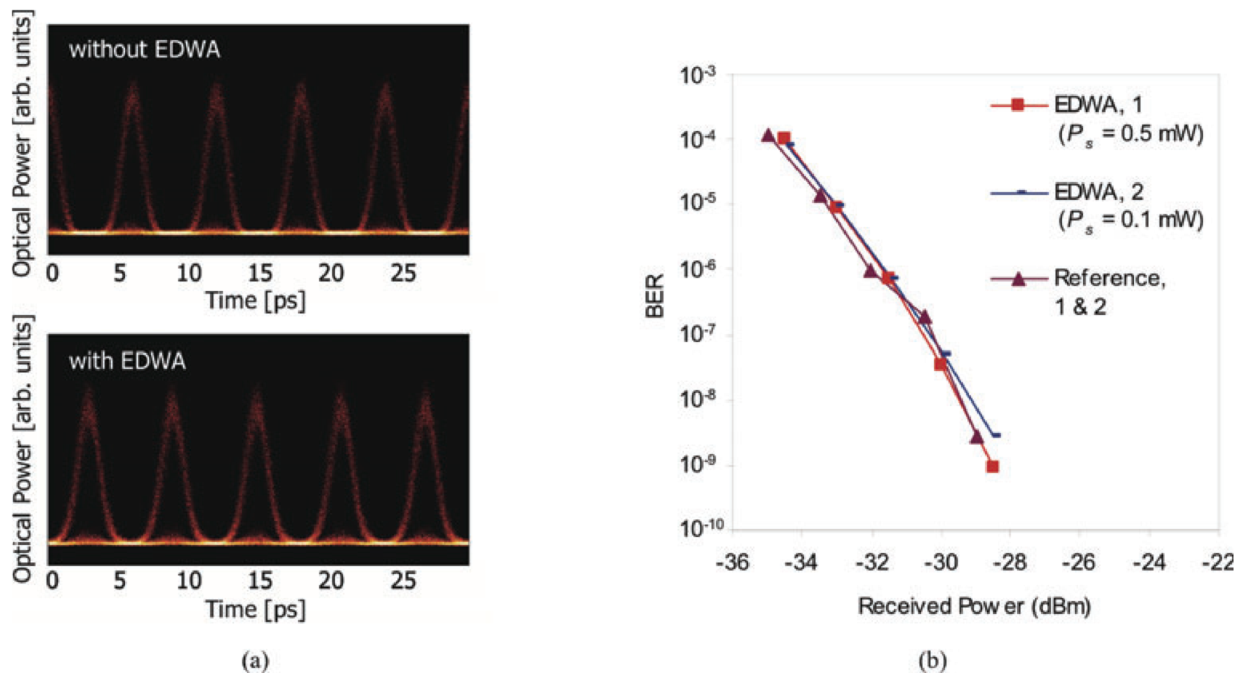

Figure 14 (online color at: www.lpr-journal.org) (a) Eye diagrams and (b) bit error rate (BER) curves for transmission experiments at 170 Gbit/s with and without (reference) EDWA included in transmission system (from [245], © 2009 Optical Society of America).

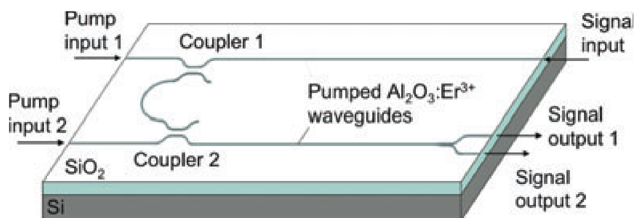

Figure 15 (online color at: www.lpr-journal.org) Illustration of planar on-chip power splitter with amplifying Er-doped waveguides (from [203], © 2010 IEEE).

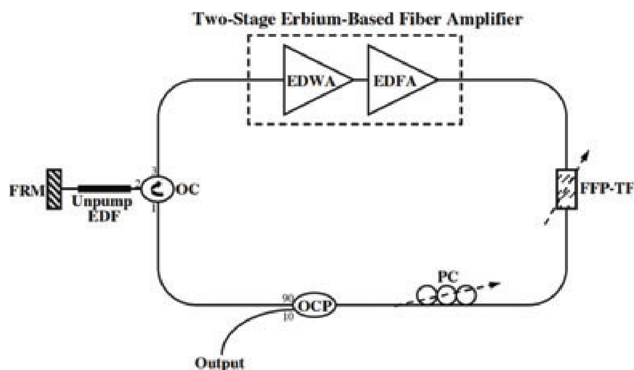

Figure 16 Experimental setup for an Er-doped fiber laser with tunable power-equalized output (from [250], © 2007 Optical Society of America).

waveguides [255] and a high-temperature sensor based on green upconversion have been investigated [172].

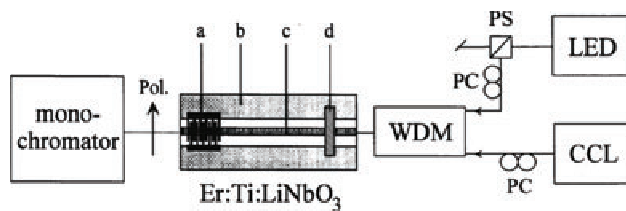

Figure 17 An acoustically tunable Er:Ti:$LiNbO_3$ wavelength filter with gain: CCL = tunable colour center laser, a = unidirectional interdigital transducer, b = 130-µm-wide acoustical waveguide, c = 7-µm-wide optical waveguide, d = acoustical wave absorber (from [252], © 1994 IEEE).

5. Er-doped waveguide lasers

Rare-earth-ion-doped dielectric lasers are of great interest for their high stability, low noise, narrow linewidth emission, broad wavelength tunability, and application as either continuous-wave (CW) or short-pulse coherent light sources. Er lasers offer emission at the frequently used wavelengths around 1.5–1.6 µm in the 3rd telecommunications window. Also a quasi phase-matched self-frequency-doubling laser emitting frequency-doubled radiation at 765.5 nm has been reported [256]. Besides, lasing on the transitions $^4I_{11/2} \rightarrow {}^4I_{13/2}$ at 2.7–2.9 µm [257] and $^4S_{3/2} \rightarrow {}^4I_{15/2}$ at 550 nm [258] has been extensively investigated. In the following sections, progress on EDWLs around 1.5–1.6 µm is surveyed, including the design of on-chip micro-resonators for EDWLs, the various approaches to CW and short-pulse lasers, and their applications.

© 2011 by WILEY-VCH Verlag GmbH & Co. KGaA, Weinheim

5.1. Resonator design

The leap from amplification of an existing signal to signal generation requires a suitable cavity structure. This includes the gain element (in this case the Er-doped waveguide) and a feedback mechanism. The losses induced by the feedback or reflection mechanism must also be sufficiently low to maintain roundtrip gain in the cavity. EDWL resonator designs can be divided into those utilizing external or off-chip reflector elements and fully-integrated cavities where lasing is achieved on the chip. A combination of both can be used, whereby one element is located off-chip.

Off-chip resonator designs include external mirrors, butt-coupled or end-deposited mirrors, and butt-coupled fibers with fiber Bragg gratings (FBGs). Advantages of these methods are the straightforward fabrication and ready availability of reflection elements, especially if a stand-alone fiber-pigtailed laser component is desired, and the ability to select and adjust the reflectivity of the cavity elements. A disadvantage with such methods is the difficult alignment and inherent sensitivity to minor misalignments. Also, the output laser signal exits the chip, hence it cannot be easily used for subsequent applications on the same chip.

Several methods have been used to fabricate on-chip laser cavities. End-reflecting mirrors can be replaced by distributed Bragg reflectors written directly into the waveguide, resulting in a distributed Bragg reflector (DBR) laser. A distributed feedback (DFB) laser is based on a distributed Bragg reflector written into the center of the waveguide. Feedback may also be achieved by means of an integrated ring resonator. An advantage of this last approach is the ability to pattern the Er-doped channel waveguide and laser cavity in a single processing step. However, a disadvantage of such ring lasers is that relatively long device lengths are required, with the result that the laser output tends to be multi-longitudinal mode. While DBR and DFB lasers require extra processing steps and an available method for patterning low-loss grating structures directly into the waveguide, they offer highly stable single-frequency operation. An advantage of each of these methods is that the laser cavity itself is highly stable, because it is imprinted on the chip. Another significant advantage is that the laser signal can either be coupled from the chip for external use or it can be used by other integrated devices and to perform other functions on the same chip. The increased level of integration is also desirable for large-scale production.

5.2. Continuous-wave lasers

Numerous CW Er-doped lasers have been realized in different host materials using the approaches described in the previous section. The performance of different lasers is compared in Table 10. The first EDWLs demonstrated in the early 1990's were based on an external butt-coupled or end-deposited mirror approach [31, 33, 130], see Fig. 18a. Figure 18b shows another external cavity configuration using fiber Bragg gratings. Examples of on-chip laser cavi-

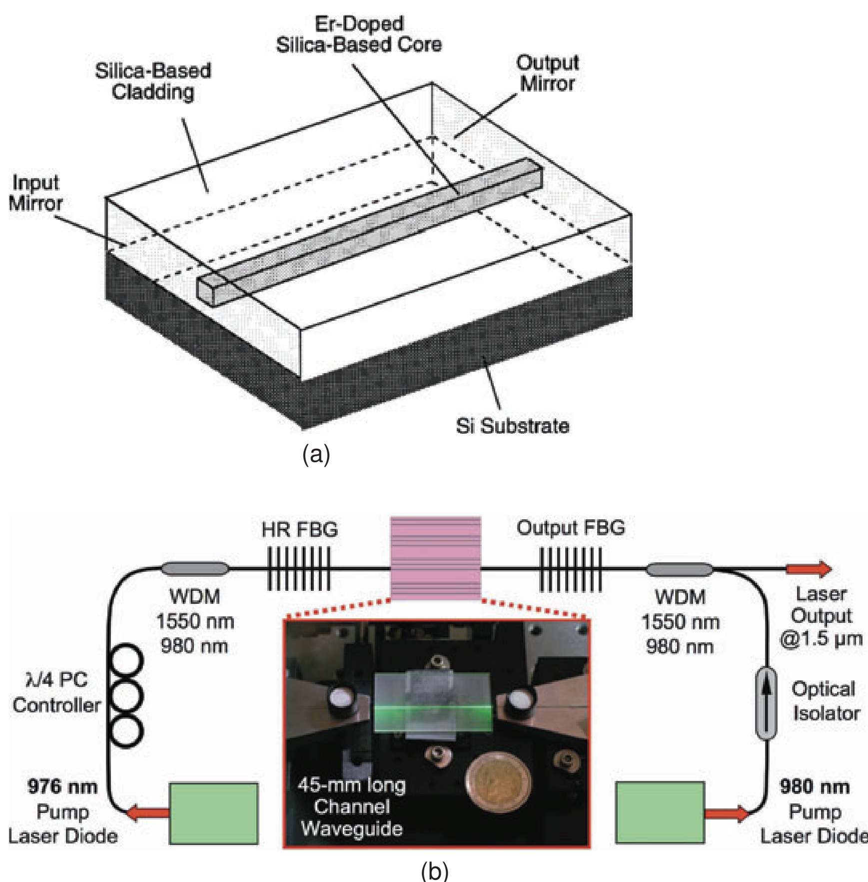

Figure 18 (online color at: www.lpr-journal.org) External-cavity CW EDWLs: (a) Illustration of an Er-doped phosphosilicate glass channel waveguide laser with end-coated mirrors. (Reprinted with permission from [31]. Copyright 1996, American Institute of Physics.); (b) illustration and photograph of experimental setup for an Er-doped waveguide FBG laser cavity (from [41], © 2008 Optical Society of America).

© 2011 by WILEY-VCH Verlag GmbH & Co. KGaA, Weinheim

Table 10 CW Er-doped and Er-, Yb-co-doped waveguide lasers.

Cavity Type	Host Material	Threshold Launched Pump Power [mW]	Maximum Output Power [mW]	Slope Efficiency vs. Launched Pump Power [%]	Ref.
External					
End-deposited mirrors	Phosphosilicate glass	49	1.2	0.81	[31]
	Zinc-silicate glass	32 to 87	19.6	1.3 to 6.5	[116]
	Ti:$LiNbO_3$	8	0.011	0.4	[33]
		13	3	3	[266]
		?	0.500	?	[268]
	BK-7 glass	150	0.40	0.55	[130]
	Phosphate glass	23/51	125/170	28	[264]
		40	130	33	[265]
Butt-coupled FBG	Oxyfluoride silicate glass	250	0.012	0.001	[269]
	Phosphate glass	85	0.8	2.0	[122]
		83	1.7	4	[270]
		190	0.7	1.1	[271]
		83 to 96	>1.0	2.0–4.0	[199]
		240	1.7	3.0	[204]
		110	30	8.4	[272]
		142	80	21	[202]
		135	22	17	[41]
		~ 150	160	46	[41]
External FBG/mirror	Phosphate glass	35	2.2	10.6	[273]
On-chip					
DBR/end-deposited mirror	Ti:$LiNbO_3$	40	5	7	[274]
	Phosphate glass	60	11	13	[275]
		50	80	26	[120]
DFB/end-deposited mirror	Ti:$LiNbO_3$	90	8	22	[263]
DBR	Phosphosilicate glass	60	0.34	~ 0.3	[259]
	Ti:$LiNbO_3$	70	1.1	2	[260]
	Al-doped germano-silicate glass	21	0.4	0.16	[276]
DFB/DBR	Ti:(Fe):$LiNbO_3$	90	8.0	22	[268]
DFB	Phosphate glass	60	4.5	2.2	[277]
		14	4.2	5.7	[42]
		?	0.37	?	[278]
	Al_2O_3	2.2^{*}	3	41.3^{**}	[46]
Ring	Phosphosilicate glass	93	0.600	0.3	[279]
	Ti:$LiNbO_3$	70	0.150	~ 0.17	[268]
	Al_2O_3	6.4	0.01	0.11	[267]
Toroidal micro-resonator	SiO_2	0.0159	0.0001	0.16	[45]
		0.0007	0.0008	23	[262]
		0.0042	0.0004	3.4	[261]

* Threshold absorbed pump power.

** Slope efficiency vs. absorbed pump power.

© 2011 by WILEY-VCH Verlag GmbH & Co. KGaA, Weinheim

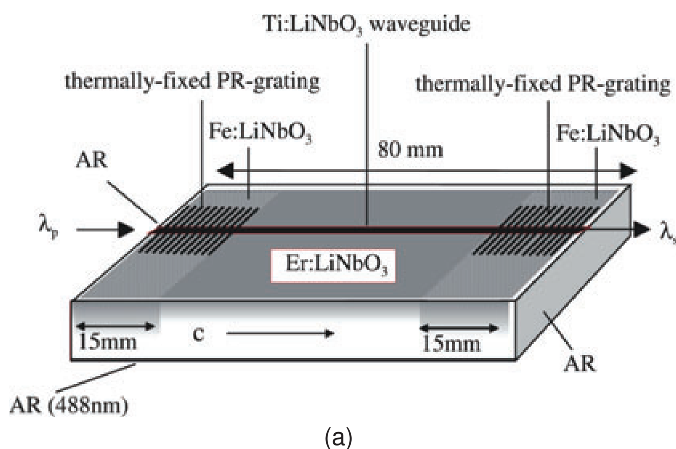

(a)

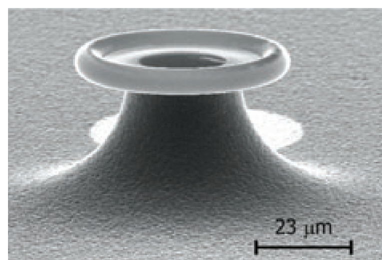

(b)

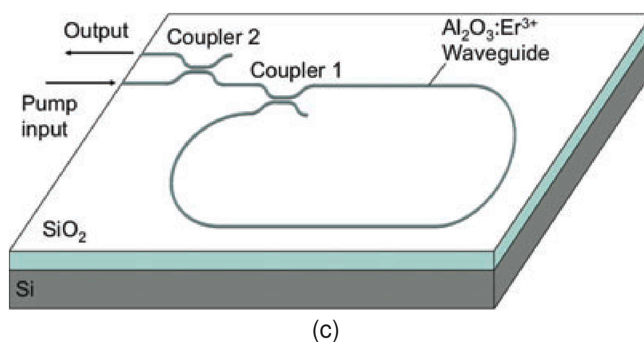

(c)

Figure 19 (online color at: www.lpr-journal.org) On-chip cavity configurations for CW EDWLs. (a) An Er:Ti:LiNbO$_3$ DBR laser (With kind permission from Springer Science+Business Media: Applied Physics B, Single-frequency Ti:Er:LiNbO$_3$ distributed Bragg reflector waveguide laser with thermally fixed photorefractive cavity, vol. 73, 2001, pg. 439, B. K. Das, H. Suche, and W. Sohler, Fig. 1). (b) SEM image of a micro-toroidal Er-doped silica glass laser (Reprinted with permission from [280]. Copyright 2006, American Institute of Physics.)., (c) Illustration of an integrated Er-doped Al$_2$O$_3$:Er^{3+} ring laser (from [267], © 2010 Optical Society of America).

ties are shown in Fig. 19a–c. A fully integrated laser was demonstrated by use of a phosphosilicate glass waveguide and a DBR cavity which also allowed for stable, single-frequency output [259]. In that specific case Bragg gratings were written using H_2 exposure and ArF eximer laser irradiation. Variations of this grating definition method have been utilized to fabricate DBR and DFB lasers, including photorefractive grating writing in Er-doped LiNbO$_3$ waveguides [260], see Fig. 19a, and interferometric exposure and etching in Er-doped phosphate glass [42]. In a novel approach, miniature toroidal Er-doped and Er-, Yb-co-doped silica lasers have been realized [45, 261], see Fig. 19b. A threshold pump power $< 1\,\mu$W, output power of 0.8 µW, and slope efficiency of 23% have been demonstrated in a micro-toroid laser with a diameter of 60 µm [262]. Such a device has highly promising implications for integration within micro- and nano-photonic circuits. However, coupling to and from the micro-toroid in an integrated manner remains a challenge which must be overcome.

In terms of laser performance, high slope efficiencies, in excess of 20%, have been demonstrated in Er:Ti:LiNbO$_3$ [263] and Er-doped phosphate glass [120, 202, 264, 265]. A slope efficiency of up to 46% using bi-directional pumping was reported in [41]. Output powers of several mW are typically reported, with a high output power of 160 mW reported in [41]. In general, the highest output powers have been achieved using an external cavity approach via fiber Bragg gratings (see Fig. 18b) or end-deposited mirrors. However an output power of 80 mW was achieved in [120] using a combination of an integrated grating structure and end-deposited mirror. While relatively high pump powers are usually required, threshold pump powers below 20 mW were reported in [33, 42, 266, 267]. High-threshold, high-output-power and low-threshold, low-output-power laser curves are compared in Fig. 20a and b, respectively. Recently, a fully-integrated, narrow-linewidth (1.7 kHz) DFB laser source emitting at 1545.2 nm with a low pump threshold of 2.2 mW and a slope efficiency of 41.3% has also been realized in Al$_2$O$_3$:Er^{3+} on silicon [46], see Figs. 21a and b.

The broad gain provided by Er in glass hosts also introduces the potential for tunable lasers. An acousto-optically tunable laser with output over the wavelength range 1530–1577 nm was reported in [268]. The principle of tunability using a ring laser and adjusting the output coupling was introduced in [267] (see Fig. 19c). In that case, multiple wavelengths in the range 1530–1557 nm were demonstrated.

5.3. Pulsed lasers

The inherently broad gain in EDWLs presents the possibility to realize short-pulse laser sources. Pulsed operation can be achieved by a number of methods, including gain-switching, mode-locking via saturable absorbers, and Q-switching by optical modulators. Integrated waveguide lasers offer high gain in short cavity lengths as compared to free-space or fiber lasers, allowing for ultra-compact devices. Furthermore, integration leads to enhanced stability.

Pioneering work on integrated Er-doped short-pulse lasers focused on LiNbO$_3$ as a host medium [35]. This material offers the advantage of integrating mode-locking and Q-switching elements directly into the laser cavity, thus

© 2011 by WILEY-VCH Verlag GmbH & Co. KGaA, Weinheim

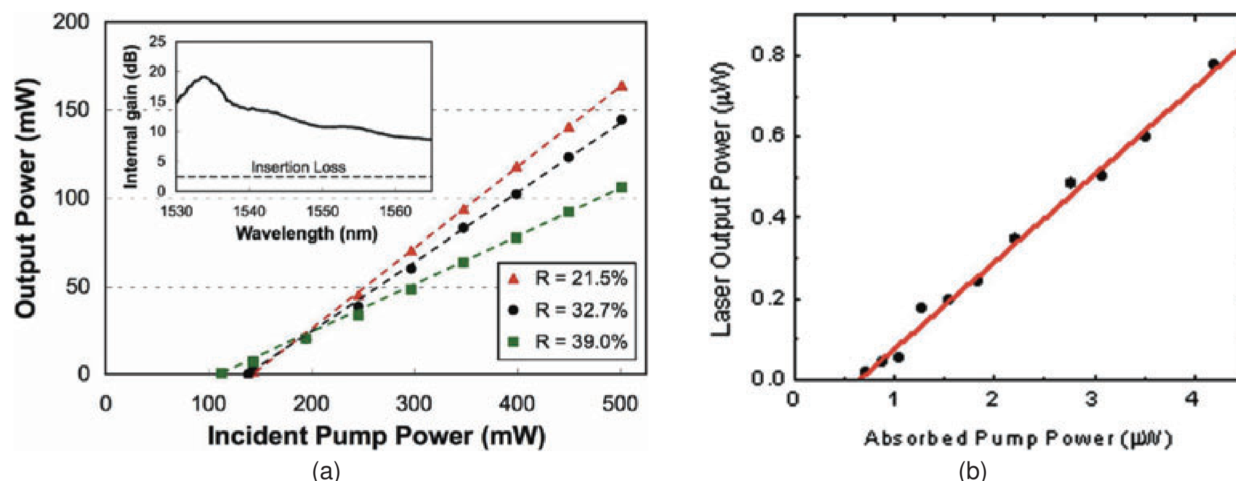

Figure 20 (online color at: www.lpr-journal.org) Laser power vs. pump power for: (a) a high-threshold, high-output-power Er-doped channel waveguide laser [41] and (b) ultra-low-threshold, low-output-power Er-doped micro-toroidal laser (Reproduced with permission from [262]. Copyright 2005, American Institute of Physics.).

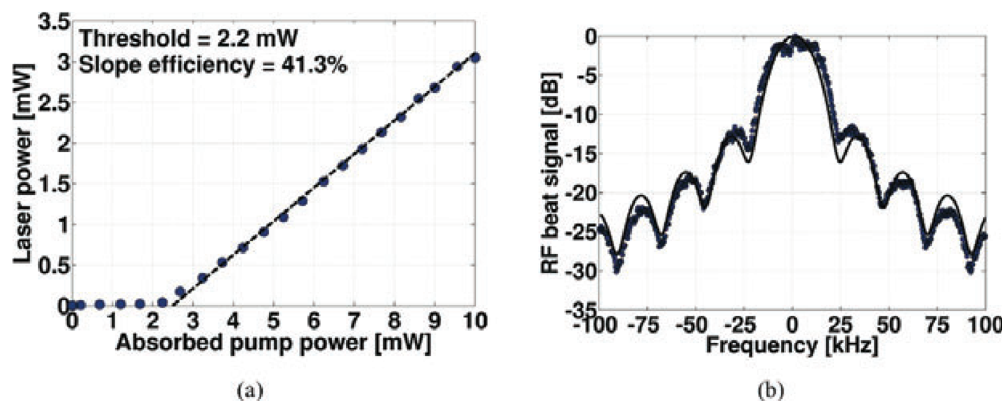

Figure 21 $Al_2O_3:Er^{3+}$ DFB laser: (a) Laser output power as a function of absorbed pump power; (b) Measured RF beat signal (circles), along with the theoretical RF power spectrum (line) which represents a Lorentzian linewidth of 1.7 kHz (from [46], © 2010 Optical Society of America).

providing a fully-monolithic solution. Mode-locking was achieved in an $Er:Ti:LiNbO_3$ waveguide laser cavity with end-deposited dielectric mirrors by means of an intracavity travelling-wave phase modulator [281]. Repetition rates of 5 GHz and pulse widths of 3.8 ps were demonstrated. A peak pulse power of 650 mW and pulse energy of 5.6 pJ was reported. A depiction of the device is shown in Fig. 22a. A fully fiber-pigtailed soliton laser source in $Er:LiNbO_3$ based on the same principle was reported in [282]. Q-switching was demonstrated in an $Er:Ti:LiNbO_3$ laser cavity using an intracavity Mach-Zehnder interferometer (MZI) amplitude modulator. A repetition rate of 2 kHz, pulse width of 100 ns, and peak pulse power of 2.4 W were demonstrated [283].

Recently, research has focused on phosphate and multi-component silicate glass waveguides for short-pulse laser applications. Sub-microsecond pulse widths were first demonstrated in a phosphosilicate glass waveguide laser in [233]. Gain switching was achieved via acousto-optic modulation of 651 nm pump light. Pulsed laser operation has also been investigated using an external-cavity approach and Er-doped phosphate glass waveguides. In [284], the cavity was formed using a butt-coupled fiber Bragg grating at one end of the waveguide and a circulator at the other. Q-switching was achieved by means of a $LiNbO_3$ electro-optic modulator (EOM). Mode-locking was demonstrated using an external semiconductor saturable absorber mirror in [121], and using a fiber-pigtailed carbon nanotube saturable absorber in [285]. The laser cavity was formed using a butt-coupled fiber mirror and the reflecting saturable absorber element in the first case (see Fig. 22b) and using a fiber-ring layout in the second case (see Fig. 22c). Repetition rates of up to 100 MHz [121], pulse widths down to 1.6 ps [285], and peak pulse powers of up to 13.5 W [284] were demonstrated in such external-cavity approaches. Recently, a more highly integrated approach to short-pulse generation was demonstrated in [286, 287]. The laser cavity was formed using an Er-doped aluminosilicate glass waveguide, an integrated reflecting mirror fabricated in P-doped silicate glass, and a butt-coupled saturable Bragg reflector, as shown in Fig. 22d. 440 fs pulses were demonstrated with a repetition rate of

© 2011 by WILEY-VCH Verlag GmbH & Co. KGaA, Weinheim

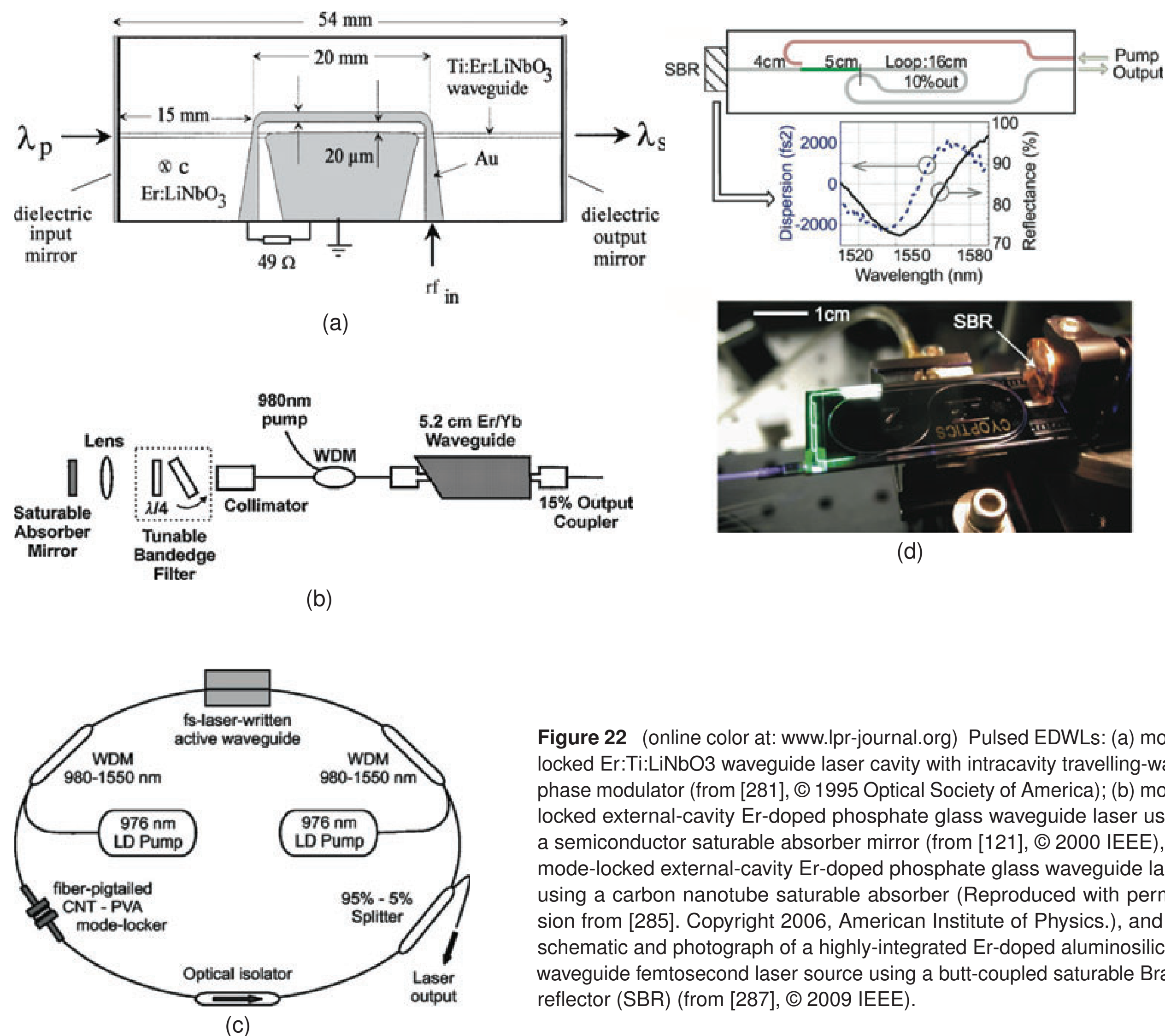

Figure 22 (online color at: www.lpr-journal.org) Pulsed EDWLs: (a) mode-locked Er:Ti:LiNbO3 waveguide laser cavity with intracavity travelling-wave phase modulator (from [281], © 1995 Optical Society of America); (b) mode-locked external-cavity Er-doped phosphate glass waveguide laser using a semiconductor saturable absorber mirror (from [121], © 2000 IEEE), (c) mode-locked external-cavity Er-doped phosphate glass waveguide laser using a carbon nanotube saturable absorber (Reproduced with permission from [285]. Copyright 2006, American Institute of Physics.), and (d) schematic and photograph of a highly-integrated Er-doped aluminosilicate waveguide femtosecond laser source using a butt-coupled saturable Bragg reflector (SBR) (from [287], © 2009 IEEE).

394 MHz. An average output power of 1.2 mW was measured for pump powers of 400 mW. Ultra-low timing jitter of 24 fs was measured, in comparison to the typically 100's of fs to ps observed in semiconductor pulsed laser sources. In addition, passive mode-locking was employed and the laser self-started, eliminating the need for complex control circuitry. Short-pulse lasers based on Er-doped waveguides and their characteristics are compared in Table 11.

5.4. Applications

Owing to their emission in the third telecom window, EDWLs could be highly useful for telecommunications applications. One specific example is a laser array providing multiple single-mode, narrow linewidth sources. The high potential of integration is that multiple devices can be fabricated within a compact chip. Arrays of single-frequency emitting lasers have been demonstrated in [42, 199, 270, 275, 277], see Fig. 23. In [42], 130-MHz linewidth sources ranging from 1533 to 1542 nm and spaced on the 25- and 100-GHz International Telecommunications Union (ITU) grid were realized. A low threshold pump power of 14 mW and output powers of up to 4.2 mW were demonstrated.

EDWLs are also of interest for many niche applications. One such example is as a highly stable, high-power integrated laser for clock circuits for satellites. Rare-earth-ion-doped polycrystalline and crystalline materials have peaked emission spectra and higher absorption and emission cross sections, thus satisfying the requirements of this and other applications which may demand higher output power with good pump efficiency and lower lasing threshold. Active microcavities are also useful for sensing applications [289]. Tunable lasers could provide multiple signal wavelengths for on-chip applications, including optical sensing in microfluidic glass channels in the same substrate. In addition, such lasers could be used for compact, hand-held medical devices. The possibility to dope with other rare-earth ions to achieve lasing over a wide wavelength range is extremely attractive.

 © 2011 by WILEY-VCH Verlag GmbH & Co. KGaA, Weinheim

Table 11 Performance comparison of pulsed Er-doped and Er-, Yb-co-doped waveguide lasers.

Laser Description	Host Material	Output wavelength(s) [nm]	Repetition Rate [GHz]	Pulse Width	Pulse Energy [μJ]	Peak Power [W]	Ref.
Gain-switched by acousto-optic modulation of pump light	Phospho-silicate glass	1608	0.018–0.060	660–2600 ns	–	0.001–0.0065	[233]
Passively mode-locked fiber ring laser	Phosphate glass	1531, 1539	0.130	116 fs	0.16	0.021*	[288]
Mode-locked by intracavity travelling-wave phase modulator	$Ti:LiNbO_3$	1532	1.441	95 ps	–	0.0015	[35]
Mode-locked by intracavity travelling-wave phase modulator	$Ti:LiNbO_3$	1602	5.124	3.8 ps	5.6×10^{-6}	0.650	[281]
Mode-locked by intracavity travelling-wave phase modulator	$Ti:LiNbO_3$	1575, 1562	5.148	7.4 ps	–	0.310	[282]
Q-switched by intracavity MZI amplitude modulator	$Ti:LiNbO_3$	1561	0.002	∼ 100 ns	0.18	2.4	[283]
Q-switched by external $LiNbO_3$ EOM	Phosphate glass	1536	0.002	200 ns	2.7	13.5	[284]
Mode-locked by external semiconductor saturable absorber mirror	Phosphate glass	1534	0.1	9.8 ps	–	0.0014*	[121]
Mode-locked by external fiber-pigtailed carbon nanotube saturable absorber	Phosphate glass	1535	0.0167	1.6 ps	–	–	[285]
Mode-locked by butt-coupled saturable Bragg reflector	Alumino-silicate glass	∼ 1558 (8.4 nm FWHM)	0.394	440 fs	–	0.0012*	[286, 287]

* Average power.

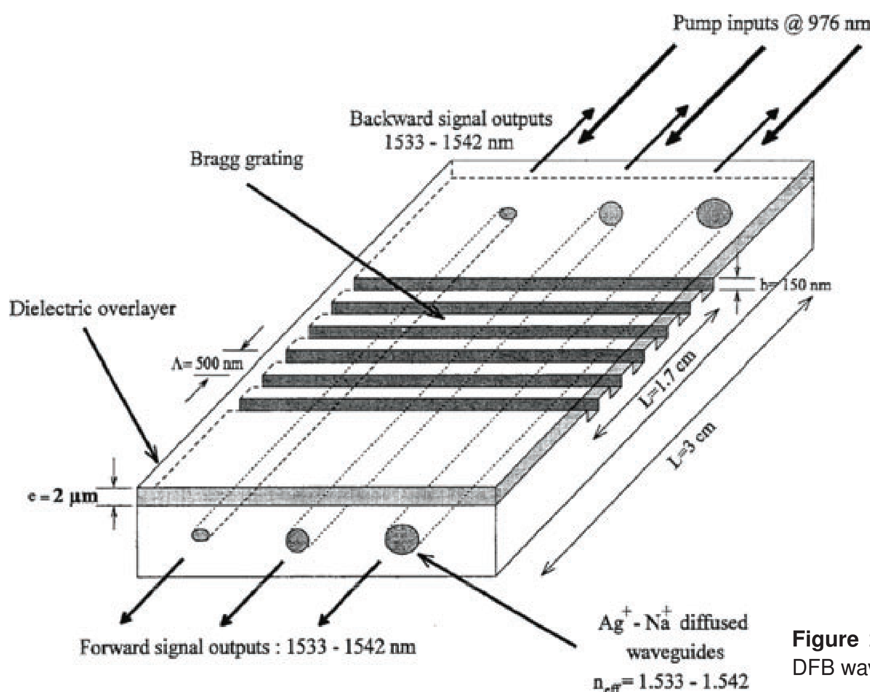

Figure 23 An Er-, Yb-co-doped phosphate glass DFB waveguide laser array (from [42], © 2003 IEEE).

6. The future: Integration of multiple active/passive functionalities on a single chip

The potential advantages of device integration are the ability to achieve high functionality in a miniature sized device and at low cost. Ideally, in integrated optics, it is desirable to combine active functions such as light emission, amplification, modulation, and detection with passive functions such as power splitting and wavelength filtering on the same chip. III-V semiconductor materials demonstrate superior optoelectronic properties, including efficient light emission and passive and active device integration in a single material system. However, integrated optics platforms such as silicon and silica-on-silicon are much more attractive than III-V semiconductors due to their significantly lower cost. III-V materials require epitaxial growth on lattice-matched substrates and are not as widely available as silicon and silica. Furthermore, a much broader fabrication knowledge base and infrastructure exists for silicon- and silica-based integrated devices. Nonetheless, active elements in the those materials remain a challenge, particularly in pure silicon, where light emission is inefficient due to its indirect bandgap. The ability to integrate active and passive devices on the same substrate allows for full optical functionality and complex photonic circuitry to be realized. An example of such a device is an integrated transceiver, whereby a signal is generated, transmitted, and detected all on the same chip. This principle is highly interesting for its application in high-speed optical interconnects. Er-doped waveguide devices may yet play a role in such applications.

Simultaneous passive and active optical device integration has been investigated in various Er-host materials. Fabrication techniques such as ion implantation and ion indiffusion inherently result in Er-activation in only certain regions of the chip. Therefore, pump and signal power are not highly attenuated by Er absorption in regions intended for passive devices. In order to facilitate gain in passive waveguide platforms, evanescent-wave amplification can be employed by simply depositing Er-doped layers as a cladding material in specific regions of the chip. This principle was utilized for amplification in silicate glass waveguides in [177]. Bonding of active and passive substrates has also been reported, using Er-, Yb-co-doped and undoped phosphate glasses [265]. Images of the bonded glass substrates are shown in Figs. 24a–c. This technique allows for separate passive and active regions. However, it fundamentally limits device design flexibility by completely separating the two regions. Selective placement of active regions has also been demonstrated in silica-based waveguides by a double PECVD deposition method [138]. Where active waveguides were required, the passive layer was etched and an Er-doped layer was deposited. The Er-doped layer was then removed in regions where it covered the passive layer. An array for testing the interfacial losses using this technique is illustrated in Fig. 25 (top). As shown in Fig. 25 (bottom), interfacial losses as low as 0.022 dB were achieved, demonstrating the practicality of this and similar methods.

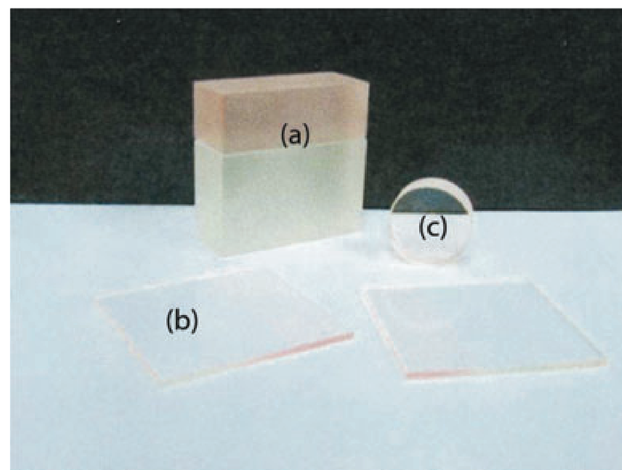

Figure 24 (online color at: www.lpr-journal.org) Active and passive optical device integration by bonding Er-doped and undoped glass substrates: (a) a hybrid preform, (b) hybrid substrates, and (c) a hybrid disk (from [265], © 2001 Optical Society of America).

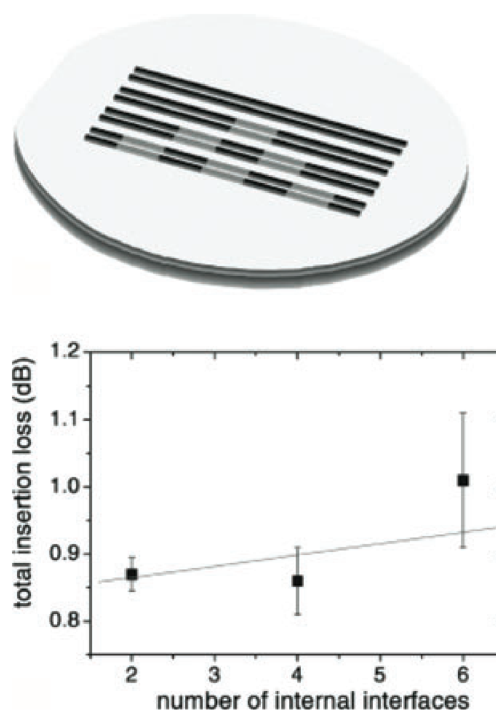

Figure 25 Illustration of double-deposition technique resulting in Er-doped and undoped regions (top) and plot of measured interfacial loss between active and passive regions (bottom) (With kind permission from Springer Science+Business Media: Applied Physics B, Planar Er- and Yb-doped amplifiers and lasers, vol. 73, 2001, pg. 435, J. Hübner, S. Guldberg-Kjær, M. Dyngaard, Y. Shen, C. L. Thomsen, S. Balslev, C. Jensen, D. Zauner, and T. Feuchter, Fig. 1.).

Significant efforts have also been focused on realizing amplification and lasing in silicon photonic circuits via Er-doping. Lasing based on electrically pumped Er-

© 2011 by WILEY-VCH Verlag GmbH & Co. KGaA, Weinheim

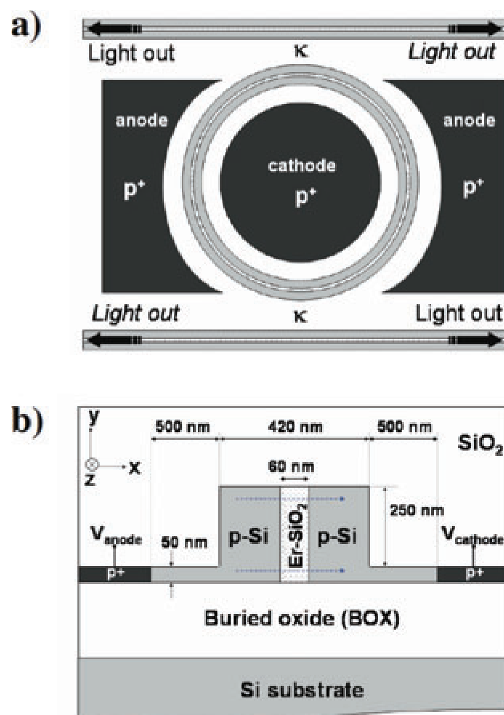

Figure 26 (a) Top view and (b) cross-section of an electrically-driven light emitting device based on Er-doped silica and silicon slot waveguides (from [290], © 2005 Optical Society of America).

doped silica-embedded silicon slot waveguides [290] and Si-nc-sensitized Er-doped silica microdisks [291] has been investigated theoretically. Figures 26a and b show an envisioned integrated slot waveguide ring laser based on the first scheme. A key challenge in such an approach is compensating for the high propagation losses (> 1 dB/cm) in the slot waveguide, which are on the same order as the highest gain demonstrated in Er-doped waveguides. Another approach involves depositing and structuring Er-doped waveguides directly on top of silicon photonic devices [292]. We recently demonstrated coupling directly from a silicon nanophotonic waveguide to a larger-cross-section $Al_2O_3{:}Er^{3+}$ waveguide via an inverse-tapered waveguide coupler, as illustrated in Fig. 27a and shown in a SEM image in Fig. 27b. A coupling loss of 2.5 dB was measured and 0.5 dB seems theoretically possible, demonstrating the feasibility of achieving net gain when coupling from silicon to EDWA and back to silicon.

In future such approaches may lead to low-cost methods of achieving simultaneously light generation and amplification in addition to high passive optical functionality on chip. Furthermore, the large selection of Er-host materials and fabrication methods enhances the potential of integrating active Er-doped waveguide devices with other on-chip technologies, including microelectronics, microfluidics and micromechanics. Integrated systems based on such combined technologies would be useful in a number of applications, including short-range optical interconnects, lab-on-a-chip devices, and hand-held devices for medicine and sensing.

7. Summary

The widespread success of Er-doped fiber amplifiers and lasers has led to a significant research effort towards compact, integrated Er-doped planar waveguide amplifiers and lasers. Numerous Er-doped host materials have been investigated, including crystalline dielectric materials, semiconductors, glasses, and polymers. Several different integrated Er-doped waveguide fabrication methods have been established, thus providing a wealth of technological solutions to choose from for designing EDWAs and EDWLs.

EDWAs have demonstrated performance similar to EDFAs. Devices have been developed which provide high gain (10s of dB) and broad gain bandwidth (net gain over 80 nm) over rather short waveguide lengths in a number of materials, each with different advantages and disadvantages

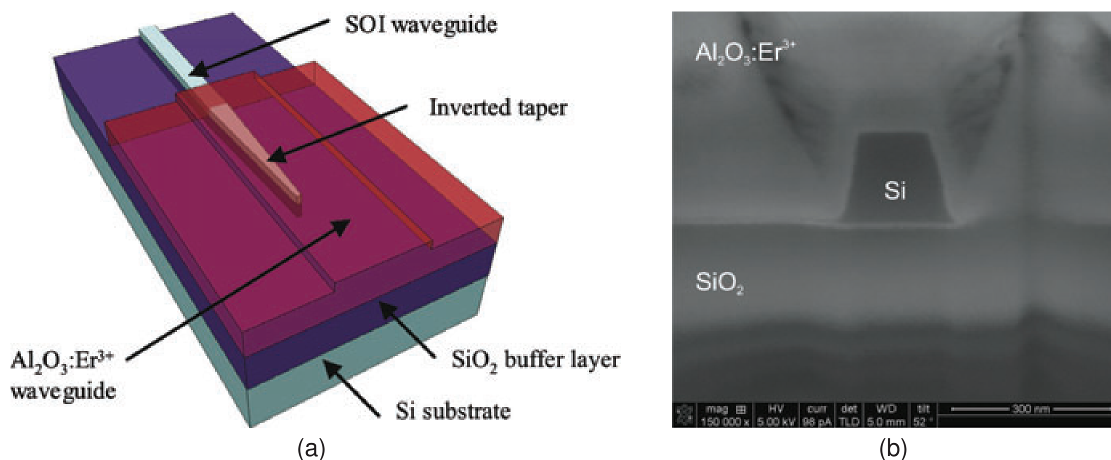

Figure 27 (online color at: www.lpr-journal.org) Monolithic integration of $Al_2O_3{:}Er^{3+}$ active waveguides and passive Si nanophotonic devices. (a) illustration of coupling from the Si waveguide to the $Al_2O_3{:}Er^{3+}$ waveguide via an inverse-taper coupler; (b) SEM cross-section of the coupling region showing the active $Al_2O_3{:}Er^{3+}$ layer directly above the Si waveguide (from [292], © 2010 Optical Society of America).

© 2011 by WILEY-VCH Verlag GmbH & Co. KGaA, Weinheim

depending on the desired application. Gain is typically carried out over lengths ranging from 1 cm to 10's of cm, the latter being reduced in size using a spiral layout. Material and design optimization has led to devices with low pump power requirements ($\leqslant$ 10 mW) with a minimal device footprint. EDWAs have been demonstrated to be highly useful for telecommunications, sensing, and other on-chip amplifying applications.

EDWLs are of great interest for their potential as compact, highly-stable and narrow-linewidth, tunable or short-pulse sources in the 1.5–1.6 μm wavelength range. Lasing has been demonstrated with Er-doped waveguides as the active gain element using a number of resonator designs. Of these, DFB lasers provide a narrow-linewidth source, while ring lasers potentially point the way towards tunable on-chip light sources. Low-threshold ($\sim$ μW), low-output-power ($\sim$ nW) micro-lasers as well as higher-threshold ($\sim$ 100 mW), high-output-power ($>$ 100 mW) laser sources are feasible. Short-pulse EDWL sources have been developed with narrow pulse width ($<$ ps) and high peak powers (up to 13.5 W) using a variety of mode-locking and Q-switching techniques and highly integrated approaches.

Future research directions include exploiting Er sensitizers and increasing functionality by integrating multiple components on the same chip. Sensitization methods which could enhance Er excitation, potentially leading to smaller, more energy-efficient devices, are currently being intensively studied. Integration of EDWAs and EDWLs with other on-chip devices will result in compact, stable, energy-efficient components for applications in telecommunications, computing, medicine, spectroscopy, and sensing.

Received: 15 July 2010, **Revised:** 4 November 2010, **Accepted:** 16 November 2010

Published online: 29 December 2010

Key words: Doped-insulator lasers and other solid state lasers, microcavity and microdisk lasers, diode-pumped lasers, resonators, cavities, amplifiers, arrays, and rings, laser applications, optical materials, integrated optics.

Jonathan D. B. Bradley completed both his B. Eng. and his M. A. Sc. degrees in Engineering Physics at McMaster University, Canada (2003 and 2005) and his Ph. D. degree in Electrical Engineering at the University of Twente, The Netherlands (2009). He was a general member and vice-chair of the IEEE Photonics Society Benelux Student Chapter (2006–2008). He currently holds a postdoctoral fellowship in the Mazur Group in the School of Engineering and Applied Sciences at Harvard University. His research focuses on the design, fabrication and characterization of advanced nonlinear nanophotonic devices.

Markus Pollnau (M. Sc. in Physics, University of Hamburg, Germany; Ph. D. in Physics, University of Bern, Switzerland) was appointed a full Professor at the University of Twente, Enschede, The Netherlands in 2004. He has contributed to $>$ 350 journal / international conference papers and six book chapters in the fields of rare-earth-ion spectroscopy, solid-state, fiber, and waveguide lasers, and integrated optical devices. He has co-chaired the Conferences on Lasers and Electro-Optics in the United States (2006/2008) and Europe (2009/2011) and served as Topical Editor for the *Journal of the Optical Society of America B*.

References

[1] R. J. Mears, L. Reekie, I. M. Jauncey, and D. N. Payne, Electron. Lett. **23**, 1026–1028 (1987).
[2] C. G. Atkins, J. F. Massicott, J. R. Armitage, R. Wyatt, B. J. Ainslie, and S. P. Craig-Ryan, Electron. Lett. **25**, 910–911 (1989).
[3] Y. Sun, J. W. Sulhoff, A. K. Srivastava, J. L. Zyskind, T. A. Strasser, J. R. Pedrazzani, C. Wolf, J. Zhou, J. B. Judkins, R. P. Espindola, and A. M. Vengsarkar, Electron. Lett. **33**, 1965–1967 (1997).
[4] P. F. Wysocki, J. B. Judkins, R. P. Espindola, M. Andrejco, and A. M. Vengsarkar, IEEE Photon. Technol. Lett. **9**, 1343–1345 (1997).
[5] C. R. Giles, and E. Desurvire, J. Lightwave Technol. **9**, 147–154 (1991).
[6] N. S. Bergano, and C. R. Davidson, J. Lightwave Technol. **14**, 1299–1308 (1996).
[7] R. J. Mears, and S. R. Baker, Opt. Quantum Electron. **24**, 517–538 (1992).
[8] K. Iwatsuki, H. Okamura, and M. Saruwatari, Electron. Lett. **26**, 2033–2035 (1990).
[9] Y. Jeong, C. Alegria, J. K. Sahu, L. Fu, M. Ibsen, C. Codemard, M. R. Mokhtar, and J. Nilsson, IEEE Photon. Technol. Lett. **16**, 756–758 (2004).
[10] J. Chow, G. Town, B. Eggleton, M. Ibsen, K. Sugden, and I. Bennion, IEEE Photon. Technol. Lett. **8**, 60–62 (1996).
[11] X. P. Dong, S. P. Li, K. S. Chiang, M. N. Ng, and B. C. B. Chu, Electron. Lett. **36**, 1609–1610 (2000).
[12] B. R. Washburn, S. A. Diddams, N. R. Newbury, J. W. Nicholson, M. F. Yan, and C. G. Jorgensen, Opt. Lett. **29**, 250–252 (2004).
[13] N. Park, J. W. Dawson, K. J. Vahala, and C. Miller, Appl. Phys. Lett. **59**, 2369–2371 (1991).
[14] G. A. Ball, and W. W. Morey, Opt. Lett. **17**, 420–422 (1992).
[15] S. Yamashita, and M. Nishihara, IEEE J. Sel. Top. Quantum Electron. **7**, 41–43 (2001).
[16] I. N. Duling, Electron. Lett. **27**, 544–545 (1991).
[17] D. J. Richardson, R. I. Laming, D. N. Payne, M. W. Phillips, and V. J. Matsas, Electron. Lett. **27**, 730–732 (1991).
[18] L. E. Nelson, D. J. Jones, K. Tamura, H. A. Haus, and E. P. Ippen, Appl. Phys. B **65**, 277–294 (1997).
[19] X. Zhou, J. Yu, M. F. Huang, Y. Shao, T. Wang, P. Magill, M. Cvijetic, L. Nelson, M. Birk, G. Zhang, S. Ten, H. B. Matthew, and S. K. Mishra, J. Lightwave Technol. **28**, 456–465 (2010).

© 2011 by WILEY-VCH Verlag GmbH & Co. KGaA, Weinheim

[20] F. Adler, K. Moutzouris, A. Leitenstorfer, H. Schnatz, B. Lipphardt, G. Grosche, and F. Tauser, Opt. Express **12**, 5872–5880 (2004).
[21] J. Cousin, P. Masselin, W. Chen, D. Boucher, S. Kassi, D. Romanini, and P. Szriftgiser, Appl. Phys. B **83**, 261–266 (2006).
[22] P. F. Wysocki, M. J. F. Digonnet, B. Y. Kim, and H. J. Shaw, J. Lightwave Technol. **12**, 550–567 (1994).
[23] J. Ma, M. Li, L. Y. Tan, Y. P. Zhou, S. Y. Yu, and Q. W. Ran, Opt. Express **17**, 15571–15577 (2009).
[24] L. Eldada, Opt. Eng. **40**, 1165–1178 (2001).
[25] Y. Vlasov, W. M. J. Green, and F. Xia, Nat. Photonics **2**, 242–246 (2008).
[26] C. Monat, P. Domachuk, and B. J. Eggleton, Nat. Photonics **1**, 106–114 (2007).
[27] R. Martínez Vázquez, R. Osellame, D. Nolli, C. Dongre, H. H. van den Vlekkert, R. Ramponi, M. Pollnau, and G. Cerullo, Lab Chip **9**, 91–96 (2009).
[28] A. Polman, J. Appl. Phys. **82**, 1–39 (1997).
[29] A. J. Kenyon, Prog. Quantum Electron. **26**, 225–284 (2002).
[30] D. R. Zimmerman, and L. H. Spiekman, J. Lightwave Technol. **22**, 63–70 (2004).
[31] T. Kitagawa, K. Hattori, M. Shimizu, Y. Ohmori, and M. Kobayashi, Electron. Lett. **27**, 334–335 (1991).
[32] T. Kitagawa, K. Hattori, K. Shuto, M. Yasu, M. Kobayashi, and M. Horiguchi, Electron. Lett. **28**, 1818–1819 (1992).
[33] R. Brinkmann, W. Sohler, and H. Suche, Electron. Lett. **27**, 415–417 (1991).
[34] R. Brinkmann, I. Baumann, M. Dinand, W. Sohler, and H. Suche, IEEE J. Quantum Electron. **30**, 2356–2360 (1994).
[35] H. Suche, L. Baumann, D. Hiller, and W. Sohler, Electron. Lett. **29**, 1111–1112 (1993).
[36] G. N. van den Hoven, R. Koper, A. Polman, C. van Dam, J. W. M. van Uffelen, and M. K. Smit, Appl. Phys. Lett. **68**, 1886–1888 (1996).
[37] H. J. van Weerden, T. H. Hoekstra, P. V. Lambeck, and T. J. A. Popma, in: Proceedings of the 8th European Conference on Integrated Optics, Stockholm, Sweden, 1997, pp. 169–172.
[38] G. Nykolak, M. Haner, P. C. Becker, J. Shmulovich, and Y. H. Wong, IEEE Photon. Technol. Lett. **5**, 1185–1187 (1993).
[39] J.-M. P. Delavaux, S. Granlund, O. Mizuhara, L. D. Tzeng, D. Barbier, M. Rattay, F. Saint, André, and A. Kevorkian, IEEE Photon. Technol. Lett. **9**, 247–249 (1997).
[40] Y. C. Yan, A. J. Faber, H. de Waal, P. G. Kik, and A. Polman, Appl. Phys. Lett. **71**, 2922–2924 (1997).
[41] G. Della Valle, A. Festa, G. Sorbello, K. Ennser, C. Cassagnetes, D. Barbier, and S. Taccheo, Opt. Express **16**, 12334–12341 (2008).
[42] S. Blaize, L. Bastard, C. Cassagnètes, and J. E. Broquin, IEEE Photon. Technol. Lett. **15**, 516–518 (2003).
[43] C. E. Chryssou, F. Di Pasquale, and C. W. Pitt, J. Lightwave Technol. **19**, 345–349 (2001).
[44] N. Daldosso, and L. Pavesi, Laser Photonics Rev. **3**, 508–534 (2009).
[45] A. Polman, B. Min, J. Kalkman, T. J. Kippenberg, and K. J. Vahala, Appl. Phys. Lett. **84**, 1037–1039 (2004).
[46] E. H. Bernhardi, H. A. G. M. van Wolferen, L. Agazzi, M. R. H. Khan, C. G. H. Roeloffzen, K. Wörhoff, M. Pollnau, and R. M. de Riddder, Opt. Lett. **35**, 2394–2396 (2010).
[47] Manlight, http://www.manlight.com/.
[48] R. S. Quimby, W. J. Miniscalco, and B. Thompson, SPIE Proc. **1581**, 72–79 (1991).
[49] T. Danger, J. Koetke, R. Brede, E. Heumann, G. Huber, and B. H. T. Chai, J. Appl. Phys. **76**, 1413–1422 (1994).
[50] M. Pollnau, W. Lüthy, H. P. Weber, K. Krämer, H. U. Güdel, and R. A. McFarlane, Appl. Phys. B **62**, 339–344 (1996).
[51] S. R. Lüthi, M. Pollnau, H. U. Güdel, and M. P. Hehlen, Phys. Rev. B **60**, 162–178 (1999).
[52] D. E. McCumber, Phys. Rev. A **134**, A299-A306 (1964).
[53] W. J. Miniscalco, and R. S. Quimby, Opt. Lett. **16**, 258–260 (1991).
[54] W. J. Miniscalco, J. Lightwave Technol. **9**, 234–250 (1991).
[55] W. L. Barnes, R. I. Laming, E. J. Tarbox, and P. R. Morkel, IEEE J. Quantum Electron. **27**, 1004–1010 (1991).
[56] C. Strohhöfer, and A. Polman, Opt. Mater. **21**, 705–712 (2003).
[57] T. H. Hoekstra, PhD thesis, University of Twente, Enschede, The Netherlands (1994).
[58] M. Dinand, and W. Sohler, IEEE J. Quantum Electron. **30**, 1267–1276 (1994).
[59] A. Kahn, H. Kühn, S. Heinrich, K. Petermann, J. D. B. Bradley, K. Wörhoff, M. Pollnau, Y. Kuzminykh, and G. Huber, J. Opt. Soc. Am. B **25**, 1850–1853 (2008).
[60] M. Pollnau, T. Graf, J. E. Balmer, W. Luthy, and H. P. Weber, Phys. Rev. A **49**, 3990–3996 (1994).
[61] S. D. Jackson, T. A. King, and M. Pollnau, Opt. Lett. **24**, 1133–1135 (1999).
[62] J. Schneider, IEEE Photon. Technol. Lett. **7**, 354–356 (1995).
[63] M. Pollnau, C. Ghisler, W. Lüthy, H. P. Weber, J. Schneider, and U. B. Unrau, Opt. Lett. **22**, 612–614 (1997).
[64] S. D. Jackson, Electron. Lett. **45**, 830–831 (2009).
[65] B. Schmaul, G. Huber, R. Clausen, B. Chai, P. Likamwa, and M. Bass, Appl. Phys. Lett. **62**, 541–543 (1993).
[66] P. C. Becker, N. A. Olsson, and J. R. Simpson, Erbium-doped fiber amplifiers: fundamentals and technology (Academic Press, San Diego, CA, 1999).
[67] M. Pollnau, and S. D. Jackson, in: Solid-State Mid-Infrared Laser Sources, Springer Series on Topics in Applied Physics, edited by I. T. Sorokina and K. L. Vodopyanov (Springer-Verlag, Berlin, Heidelberg, 2003), pp. 219–253.
[68] T. H. Hoekstra, P. V. Lambeck, H. Albers, and T. J. A. Popma, Electron. Lett. **29**, 581–583 (1993).
[69] M. Pollnau, IEEE J. Quantum Electron. **39**, 350–357 (2003).
[70] M. P. Hehlen, N. J. Cockroft, T. R. Gosnell, A. J. Bruce, G. Nykolak, and J. Shmulovich, Opt. Lett. **22**, 772–774 (1997).
[71] P. Blixt, J. Nilsson, T. Carlnäs, and B. Jaskorzynska, IEEE Photon. Technol. Lett. **3**, 996–998 (1991).
[72] B. Pálsdóttir, and C. C. Larsen, Dipole-dipole model for upconversion and fluorescence lifetime in erbium doped fibers, in: Optical Amplifiers and Their Applications, OSA Technical Digest Series, Breckenridge, CO, 1994, paper ThB5, pp. 1–3.
[73] G. N. van den Hoven, E. Snoeks, A. Polman, C. van Dam, J. W. M. van Uffelen, and M. K. Smit, J. Appl. Phys. **79**, 1258–1266 (1996).
[74] L. Agazzi, K. Wörhoff, A. Kahn, H. Scheife, G. Huber, and M. Pollnau, Influence of static and migration-accelerated energy-transfer upconversion on amplifier performance in Al_2O_3:Er^{3+}, submitted (2011).

© 2011 by WILEY-VCH Verlag GmbH & Co. KGaA, Weinheim

[75] J. D. B. Bradley, L. Agazzi, D. Geskus, F. Ay, K. Wörhoff, and M. Pollnau, J. Opt. Soc. Am. B **27**, 187–196 (2010).
[76] T. Ohtsuki, S. Honkanen, S. I. Najafi, and N. Peyghambarian, J. Opt. Soc. Am. B **14**, 1838–1845 (1997).
[77] S. Taccheo, G. Sorbello, S. Longhi, and P. Laporta, Opt. Quantum Electron. **31**, 249–262 (1999).
[78] B. C. Hwang, S. B. Jiang, T. Luo, J. Watson, G. Sorbello, and N. Peyghambarian, J. Opt. Soc. Am. B **17**, 833–839 (2000).
[79] E. Snoeks, G. N. van den Hoven, A. Polman, B. Hendriksen, M. B. J. Diemeer, and F. Priolo, J. Opt. Soc. Am. B **12**, 1468–1474 (1995).
[80] P. S. Golding, S. D. Jackson, T. A. King, and M. Pollnau, Phys. Rev. B **62**, 856–864 (2000).
[81] F. D. Patel, S. DiCarolis, P. Lum, S. Venkatesh, and J. N. Miller, IEEE Photon. Technol. Lett. **16**, 2607–2609 (2004).
[82] G. Della Valle, S. Taccheo, G. Sorbello, E. Cianci, V. Foglietti, and R. Laporta, Electron. Lett. **42**, 632–633 (2006).
[83] A. J. Kenyon, P. F. Trwoga, M. Federighi, and C. W. Pitt, J. Phys. Condens. Matter. **6**, 6383–6383 (1994).
[84] M. Fujii, M. Yoshida, Y. Kanzawa, S. Hayashi, and K. Yamamoto, Appl. Phys. Lett. **71**, 1198–1200 (1997).
[85] P. G. Kik, and A. Polman, J. Appl. Phys. **88**, 1992–1998 (2000).
[86] G. Franzò, V. Vinciguerra, and F. Priolo, Appl. Phys. A **69**, 3–12 (1999).
[87] N. Daldosso, D. Navarro-Urrios, M. Melchiorri, L. Pavesi, C. Sada, F. Gourbilleau, and R. Rizk, Appl. Phys. Lett. **88**, 161901/1–3 (2006).
[88] I. Izeddin, T. Gregorkiewicz, and M. Fujii, Physica E **38**, 144–147 (2007).
[89] N. Daldosso, D. Navarro-Urrios, M. Melchiorri, L. Pavesi, F. Gourbilleau, M. Carrada, R. Rizk, C. García, P. Pellegrino, B. Garrido, and L. Cognolato, Appl. Phys. Lett. **86**, 261103/1–3 (2005).
[90] W. H. Loh and A. J. Kenyon, IEEE Photon. Technol. Lett., **18**, 289–291 (2006).
[91] D. Pacifici, G. Franzo, F. Priolo, F. Iacona, and L. Dal Negro, Phys. Rev. B **67**, 245301/1–13 (2003).
[92] O. Savchyn, F. R. Ruhge, P. G. Kik, R. M. Todi, K. R. Coffey, H. Nukala, and H. Heinrich, Phys. Rev. B **76**, 195419/1–10 (2007).
[93] I. Izeddin, D. Timmerman, T. Gregorkiewicz, A. S. Moskalenko, A. A. Prokofiev, I. N. Yassievich, and M. Fujii, Phys. Rev. B **78**, 035327/1–14 (2008).
[94] A. J. Kenyon, M. Wojdak, I. Ahmad, W. H. Loh, and C. J. Oton, Phys. Rev. B **77**, 035318/1–9 (2008).
[95] D. Navarro-Urrios, A. Pitanti, N. Daldosso, F. Gourbilleau, L. Khomenkova, R. Rizk, and L. Pavesi, Physica E **41**, 1029–1033 (2009).
[96] J. D. B. Bradley, F. Ay, K. Wörhoff, and M. Pollnau, Appl. Phys. B **89**, 311–318 (2007).
[97] S. Bär, H. Scheife, K. Petermann, and G. Huber, in: Rare Earth Oxide Thin Films: Growth, Characterization, and Applications, Topics in Applied Physics, edited by M. Fanciulli and G. Scarel (Springer-Verlag, Berlin, 2007), pp. 401–422.
[98] G. Facchini, A. Zappettini, A. Canali, M. Martinelli, G. Gabetta, and G. Tallarida, Opt. Mater. **17**, 251–254 (2001).
[99] M. Szachowicz, S. Tascu, M.-F. Joubert, P. Moretti, and M. Nikl, Opt. Mater. **28**, 162–166 (2006).
[100] S. García-Revilla, R. Valiente, Y. E. Romanyuk, and M. Pollnau, J. Lumin. **128**, 934–936 (2008).
[101] J. M. Zavada, and D. H. Zhang, Solid-State Electron. **38**, 1285–1293 (1995).
[102] F. Priolo, G. Franzò, S. Coffa, A. Polman, S. Libertino, R. Barklie, and D. Carey, J. Appl. Phys. **78**, 3874–3882 (1995).
[103] G. Franzò, S. Coffa, F. Priolo, and C. Spinella, J. Appl. Phys. **81**, 2784–2793 (1997).
[104] S. Lanzerstorfer, L. Palmetshofer, W. Jantsch, and J. Stimmer, Appl. Phys. Lett. **72**, 809–811 (1998).
[105] A. J. Kenyon, Semicond. Sci. Technol. **20**, R65-R84 (2005).
[106] J. Lee, J. H. Shin, and N. Park, J. Lightwave Technol. **23**, 19–25 (2005).
[107] L. H. Slooff, A. Polman, M. P. O. Wolbers, F. van Veggel, D. N. Reinhoudt, and J. W. Hofstraat, J. Appl. Phys. **83**, 497–503 (1998).
[108] A. Q. Le Quang, R. Hierle, J. Zyss, I. Ledoux, G. Cusmai, R. Costa, A. Barberis, and S. M. Pietralunga, Appl. Phys. Lett. **89**, 141124/1–3 (2006).
[109] D. Zhang, C. Chen, C. M. Chen, C. S. Ma, D. M. Zhang, S. Bo, and Z. Zhen, Appl. Phys. Lett. **91**, 161109/1–3 (2007).
[110] J. Yang, M. B. J. Diemeer, D. Geskus, G. Sengo, M. Pollnau, and A. Driessen, Opt. Lett. **34**, 473–475 (2009).
[111] C. Chen, D. Zhang, T. Li, D. M. Zhang, L. M. Song, and Z. Zhen, Appl. Phys. Lett. **94**, 041119/1–3 (2009).
[112] J. Yang, M. B. J. Diemeer, C. Grivas, G. Sengo, A. Driessen, and M. Pollnau, Laser Phys. Lett. **7**, 650–656 (2010).
[113] C. Grivas, J. Yang, M. B. J. Diemeer, A. Driessen, and M. Pollnau, Opt. Lett. **35**, 1983–1985 (2010).
[114] K. Hattori, T. Kitagawa, M. Oguma, Y. Ohmori, and M. Horiguchi, Electron. Lett. **30**, 856–857 (1994).
[115] D. Barbier, M. Rattay, F. Saint, André, G. Clauss, M. Trouillon, A. Kevorkian, J.-M. P. Delavaux, and E. Murphy, IEEE Photon. Technol. Lett. **9**, 315–317 (1997).
[116] P. M. Peters, D. S. Funk, A. P. Peskin, D. L. Veasey, N. A. Sanford, S. N. Houde-Walter, and J. S. Hayden, Appl. Opt. **38**, 6879–6886 (1999).
[117] K. Ennser, S. Taccheo, T. Rogowski, and J. Shmulovich, Opt. Express **14**, 10307–10312 (2006).
[118] T. Ohtsuki, N. Peyghambarian, S. Honkanen, and S. I. Najafi, , J. Appl. Phys. **78**, 3617–3621 (1995).
[119] A. Shooshtari, P. Meshkinfam, T. Touam, M. P. Andrews, and S. I. Najafi, Opt. Eng. **37**, 1188–1192 (1998).
[120] D. L. Veasey, D. S. Funk, N. A. Sanford, and J. S. Hayden, Appl. Phys. Lett. **74**, 789–791 (1999).
[121] E. R. Thoen, E. M. Koontz, D. J. Jones, D. Barbier, F. X. Kärtner, E. P. Ippen, and L. A. Kolodziejski, IEEE Photon. Technol. Lett. **12**, 149–151 (2000).
[122] G. Sorbello, S. Taccheo, P. Laporta, O. Svelto, E. Cianci, V. Foglietti, S. Jiang, and N. Peyghambarian, Electron. Lett. **37**, 1014–1015 (2001).
[123] F. Gardillou, L. Bastard, and J. E. Broquin, Appl. Phys. Lett. **85**, 5176–5178 (2004).
[124] K. Liu, and E. Y. B. Pun, Opt. Commun. **273**, 413–420 (2007).
[125] I. Vasilief, S. Guy, B. Jacquier, B. Boulard, Y. P. Gao, C. Duverger, H. Haquin, V. Nazabal, J. L. Adam, M. Couchaud, L. Fulbert, C. Cassagnettes, F. Rooms, and D. Barbier, Appl. Opt. **44**, 4678–4683 (2005).
[126] R. Serna, and C. N. Afonso, Appl. Phys. Lett. **69**, 1541–1543 (1996).
[127] C. E. Chryssou, and C. W. Pitt, IEEE J. Quantum Electron. **34**, 282–285 (1998).

© 2011 by WILEY-VCH Verlag GmbH & Co. KGaA, Weinheim

[128] S. Musa, H. J. van Weerden, T. H. Yau, and P. V. Lambeck, IEEE J. Quantum. Electron. **36**, 1089–1097 (2000).
[129] K. Solehmainen, M. U. Kapulainen, P. Heimala, and K. Polamo, IEEE Photon. Technol. Lett. **16**, 194–196 (2004).
[130] T. Feuchter, E. K. Mwarania, J. Wang, L. Reekie, and J. S. Wilkinson, IEEE Photon. Technol. Lett. **4**, 542–544 (1992).
[131] J. Shmulovich, A. Wong, Y. H. Wong, P. C. Becker, A. J. Bruce, and R. Adar, Electron. Lett. **28**, 1181–1182 (1992).
[132] P. Camy, J. E. Román, F. W. Willems, M. Hempstead, J. C. van der Plaats, C. Prel, A. Béguin, A. M. J. Koonen, J. S. Wilkinson, and C. Lerminiaux, Electron. Lett. **32**, 321–323 (1996).
[133] R. N. Ghosh, J. Shmulovich, C. F. Kane, M. R. X. de Barros, G. Nykolak, A. J. Bruce, and P. C. Becker, IEEE Photon. Technol. Lett. **8**, 518–520 (1996).
[134] C. Strohhöfer, S. Capecchi, J. Fick, A. Martucci, G. Brusatin, and M. Guglielmi, Thin Solid Films **326**, 99–105 (1998).
[135] X. Orignac, D. Barbier, X. M. Du, R. M. Almeida, O. McCarthy, and E. Yeatman, Opt. Mater. **12**, 1–18 (1999).
[136] J. Fick, A. Martucci, and M. Guglielmi, J. Sol-Gel Sci. Technol. **19**, 573–576 (2000).
[137] Y. B. Choi, S. H. Cho, and D. C. Moon, Opt. Lett. **25**, 263–265 (2000).
[138] J. Hübner, S. Guldberg-Kjær, M. Dyngaard, Y. Shen, C. L. Thomsen, S. Balslev, C. Jensen, D. Zauner, and T. Feuchter, Appl. Phys. B **73**, 435–438 (2001).
[139] W. Huang, R. R. A. Syms, E. M. Yeatman, M. M. Ahmad, T. V. Clapp, and S. M. Ojha, IEEE Photon. Technol. Lett. **14**, 959–961 (2002).
[140] L. Zampedri, G. C. Righini, H. Portales, S. Pelli, G. N. Conti, M. Montagna, M. Mattarelli, R. R. Gonçalves, M. Ferrari, A. Chiasera, M. Bouazaoui, and C. Armellini, J. Non-Cryst. Solids **345–46**, 580–584 (2004).
[141] S. Banerjee, C. C. Baker, A. J. Steckl, and D. Klotzkin, J. Lightwave Technol. **23**, 1342–1349 (2005).
[142] R. R. Thomson, H. T. Bookey, H. Ur-Rehman, S. Liu, N. Suyal, and A. K. Kar, J. Lightwave Technol. **23**, 4249–4256 (2005).
[143] P. T. Nga, C. Barthou, P. Benalloul, P. N. Thang, L. N. Chung, P. V. Hoi, L. V. Luat, and P. T. Cuong, J. Non-Cryst. Solids **352**, 2385–2389 (2006).
[144] S. Berneschi, M. Bettinelli, M. BrenCi, R. Dall'Igna, G. N. Conti, S. Pelli, B. Profilo, S. Sebastiani, A. Speghini, and G. C. Righini, Opt. Mater. **28**, 1271–1275 (2006).
[145] A. P. Caricato, A. Fazzi, A. Jha, A. Kar, G. Leggieri, A. Luches, M. Martino, F. Romano, S. Shen, M. Taghizadeh, R. Thomson, and T. Tunno, Opt. Mater. **29**, 1166–1170 (2007).
[146] M. M. Abouelleil, G. A. Ball, W. L. Nighan, and D. J. Opal, Opt. Lett. **16**, 1949–1951 (1991).
[147] T. T. Fernandez, G. Della Valle, R. Osellame, G. Jose, N. Chiodo, A. Jha, and P. Laporta, Opt. Express **16**, 15198–15205 (2008).
[148] P. Fournier, P. Meshkinfam, M. A. Fardad, M. P. Andrews, and S. I. Najafi, Electron. Lett. **33**, 293–295 (1997).
[149] D. Barbier, P. Bruno, C. Cassagnetes, M. Trouillon, R. L. Hyde, A. Kevorkian, and J. M. P. Delavaux, Net gain of 27 dB with a 8.6-cm-long Er/Yb-doped glass-planar-amplifier, in: Optical Fiber Communication Conference and Exhibit, Technical Digest, San Jose, CA, 1998, Paper TuH5, pp. 45–46.
[150] M. Krishnaswamy, J. N. McMullin, B. P. Keyworth, and J. S. Hayden, Opt. Mater. **6**, 287–292 (1996).
[151] T. T. Van and J. P. Chang, Appl. Phys. Lett. **87**, 0011907/1–3 (2005).
[152] M. Kohls, T. Schmidt, H. Katschorek, L. Spanhel, G. Müller, N. Mais, A. Wolf, and A. Forchel, Adv. Mater. **11**, 288–292 (1999).
[153] K. Hattori, T. Kitagawa, M. Oguma, M. Wada, J. Temmyo, and M. Horiguchi, Electron. Lett. **29**, 357–359 (1993).
[154] X. Multone, Y. Luo, and P. Hoffmann, Mater. Sci. Eng. B **146**, 35–40 (2008).
[155] M. Mahnke, S. Wiechmann, H. J. Heider, O. Blume, and J. Müller, AEU Int. J. Electron. Commun. **55**, 342–348 (2001).
[156] K. Shuto, K. Hattori, T. Kitagawa, Y. Ohmori, and M. Horiguchi, Electron. Lett. **29**, 139–141 (1993).
[157] H. S. Han, S. Y. Seo, J. H. Shin, and N. Park, Appl. Phys. Lett. **81**, 3720–3722 (2002).
[158] R. Serna, J. M. Ballesteros, M. J. de Castro, J. Solis, and C. N. Afonso, J. Appl. Phys. **84**, 2352–2354 (1998).
[159] J. Remsa, M. Jelinek, T. Kocourek, J. Oswald, V. Studnicka, M. Cernansky, F. Uherek, and M. Jelinek, Appl. Surf. Sci. **255**, 5292–5294 (2009).
[160] M. B. Korzenski, P. Lecoeur, B. Mercey, P. Camy, and J.-L. Doualan, Appl. Phys. Lett. **78**, 1210–1212 (2001).
[161] A. O. G. Dikovska, P. A. Atanasov, M. Jiménez de Castro, A. Perea, J. Gonzalo, C. N. Afonso, and J. García López, Thin Solid Films **500**, 336–340 (2006).
[162] O. Pons-Y-Moll, J. Perriere, E. Millon, R. M. Defourneau, D. Defourneau, B. Vincent, A. Essahlaoui, A. Boudrioua, and W. Seiler, J. Appl. Phys. **92**, 4885–4890 (2002).
[163] S. Komuro, T. Katsumata, T. Morikawa, X. Zhao, H. Isshiki, and Y. Aoyagi, Appl. Phys. Lett. **76**, 3935–3937 (2000).
[164] K. Wörhoff, J. D. B. Bradley, F. Ay, D. Geskus, T. P. Blauwendraat, and M. Pollnau, IEEE J. Quantum Electron. **45**, 454–461 (2009).
[165] S. Yerci, R. Li, S. O. Kucheyev, T. van Buuren, S. N. Basu, and L. Dal Negro, IEEE J. Sel. Top. Quantum Electron. **16**, 114–123 (2010).
[166] R. Schermer, W. Berglund, C. Ford, R. Ramberg, and A. Gopinath, IEEE J. Quantum Electron. **39**, 154–159 (2003).
[167] J. Shmulovich, A. J. Bruce, G. Lenz, P. B. Hansen, T. N. Nielsen, D. J. Muehlner, G. A. Bogert, I. Brener, E. J. Laskowski, A. Paunescu, I. Ryazansky, D. C. Jacobson, and A. E. White, Integrated planar waveguide amplifier with 15 dB net gain at 1550 nm, in: Optical Fiber Communication Conference, Technical Digest, San Diego, CA, 1999, paper PD42, pp. 1–3.
[168] Q. Song, J. S. Gao, X. Y. Wang, H. Chen, T. T. Wang, X. M. Zheng, C. R. Li, and C. L. Song, Opt. Express **15**, 3948–3954 (2007).
[169] Q. Song, J. S. Gao, X. Y. Wang, H. Chen, X. M. Zheng, T. T. Wang, C. R. Li, and C. L. Song, Opt. Eng. **46**, 040509/1–3 (2007).
[170] Y. Kondo, M. Ono, J. Kageyama, H. Hayashi, M. Reyes, and N. Sugimoto, Electron. Lett. **41**, 317–318 (2005).
[171] S. I. Seok, and M. A. Lim, J. Am. Ceram. Soc. **88**, 2380–2384 (2005).
[172] B. Dong, T. Yang, and M. K. Lei, Sens. Actuators B **123**, 667–670 (2007).

© 2011 by WILEY-VCH Verlag GmbH & Co. KGaA, Weinheim

[173] R. M. Almeida, X. M. Du, D. Barbier, and X. Orignac, J. Sol-Gel Sci. Technol. **14**, 209–216 (1999).
[174] E. M. Yeatman, M. M. Ahmad, O. McCarthy, A. Vannucci, P. Gastaldo, D. Barbier, D. Mongardien, and C. Moronvalle, Opt. Commun. **164**, 19–25 (1999).
[175] A. Laliotis, and E. M. Yeatman, J. Lightwave Technol. **25**, 1613–1620 (2007).
[176] W. Huang, and R. R. A. Syms, J. Lightwave Technol. **21**, 1339–1349 (2003).
[177] H. S. Tang, Y. G. Li, Y. W. Zhang, Y. F. Li, H. Li, X. Tu, X. Wu, L. Y. Liu, and L. Xu, Opt. Express **16**, 9844–9849 (2008).
[178] S. X. Shen, and A. Jha, Opt. Mater. **25**, 321–333 (2004).
[179] N. D. Psaila, R. R. Thomson, H. T. Bookey, A. K. Kar, N. Chiodo, R. Osellame, G. Cerullo, A. Jha, and S. Shen, Appl. Phys. Lett. **90**, 131102/1–3 (2007).
[180] L. H. Slooff, M. J. A. de Dood, A. van Blaaderen, and A. Polman, J. Non-Cryst. Solids **296**, 158–164 (2001).
[181] A. Bahtat, M. Bouazaoui, M. Bahtat, and J. Mugnier, Opt. Commun. **111**, 55–60 (1994).
[182] P. Jenouvrier, G. Boccardi, J. Fick, A.-M. Jurdyc, and M. Langlet, J. Lumin. **113**, 291–300 (2005).
[183] H. Guo, W. Zhang, L. Lou, A. Brioude, and J. Mugnier, Thin Solid Films **458**, 274–280 (2004).
[184] S. W. Roberts, G. J. Parker, and M. Hempstead, Opt. Mater. **6**, 99–102 (1996).
[185] R. Serna, C. N. Afonso, J. M. Ballesteros, and A. Zschocke, Appl. Surf. Sci. **110**, 524–527 (1997).
[186] R. Serna, M. J. de Castro, J. A. Chaos, C. N. Afonso, and I. Vickridge, Appl. Phys. Lett. **75**, 4073–4075 (1999).
[187] R. Serna, M. J. de Castro, J. A. Chaos, A. Suárez-Garcia, C. N. Afonso, M. Fernandez, and I. Vickridge, J. Appl. Phys. **90**, 5120–5125 (2001).
[188] A. Suárez-García, R. Serna, M. J. de Castro, C. N. Afonso, and I. Vickridge, Appl. Phys. Lett. **84**, 2151–2153 (2004).
[189] L. G. Kou, D. C. Hall, C. Strohhöfer, A. Polman, T. Zhang, R. M. Kolbas, R. D. Heller, and R. D. Dupuis, IEEE J. Sel. Top. Quantum Electron. **8**, 880–890 (2002).
[190] J. H. Shin, R. Serna, G. N. van den Hoven, A. Polman, W. G. J. H. M. van Sark, and A. M. Vredenberg, Appl. Phys. Lett. **68**, 46–48 (1996).
[191] A. Polman, G. N. van den Hoven, J. S. Custer, J. H. Shin, R. Serna, and P. F. A. Alkemade, J. Appl. Phys. **77**, 1256–1262 (1995).
[192] C. Strohhöfer, P. G. Kik, and A. Polman, J. Appl. Phys. **88**, 4486–4490 (2000).
[193] Y. Lebour, D. Navarro-Urrios, P. Pellegrino, G. Sarrabayrouse, L. Pavesi, and B. Garrido, Physica E **41**, 1044–1047 (2009).
[194] R. R. Thomson, H. T. Bookey, N. Psaila, S. Campbell, D. T. Reid, S. X. Shen, A. Jha, and A. K. Kar, IEEE Photon. Technol. Lett. **18**, 1515–1517 (2006).
[195] R. Osellame, S. Taccheo, G. Cerullo, M. Marangoni, D. Polli, R. Ramponi, P. Laporta, and S. De Silvestri, Electron. Lett. **38**, 964–965 (2002).
[196] R. R. Thomson, N. D. Psaila, S. J. Beecher, and A. K. Kar, Opt. Express **18**, 13212–13219 (2010).
[197] K. Liu, E. Y. B. Pun, T. C. Sum, A. A. Bettiol, J. A. van Kan, and F. Watt, Appl. Phys. Lett. **84**, 684–686 (2004).
[198] S. F. Wong, E. Y. B. Pun, and P. S. Chung, IEEE Photon. Technol. Lett. **14**, 80–82 (2002).
[199] G. Jose, G. Sorbello, S. Taccheo, E. Cianci, V. Foglietti, and P. Laporta, J. Non-Cryst. Solids **322**, 256–261 (2003).
[200] K. Liu, and E. Y. B. Pun, Appl. Opt. **43**, 3179–3184 (2004).
[201] Y. Tan, F. Chen, L. L. Hu, P. F. Xing, Y. X. Chen, X. L. Wang, and K. M. Wang, J. Phys. D: Appl. Phys. **40**, 6545–6548 (2007).
[202] G. Della Valle, S. Taccheo, R. Osellame, A. Festa, G. Cerullo, and P. Laporta, Opt. Express **15**, 3190–3194 (2007).
[203] J. D. B. Bradley, R. Stoffer, A. Bakker, L. Agazzi, F. Ay, K. Wörhoff, and M. Pollnau, IEEE Photon. Technol. Lett. **22**, 278–280 (2010).
[204] S. Taccheo, G. Della Valle, R. Osellame, G. Cerullo, N. Chiodo, P. Laporta, O. Svelto, A. Killi, U. Morgner, M. Lederer, and D. Kopf, Opt. Lett. **29**, 2626–2628 (2004).
[205] F. Di Pasquale, and M. Federighi, IEEE J. Quantum Electron. **30**, 2127–2131 (1994).
[206] C. Lester, A. Bjarklev, T. Rasmussen, and P. G. Dinesen, J. Lightwave Technol. **13**, 740–743 (1995).
[207] A. Shooshtari, T. Touam, and S. I. Najafi, Opt. Quantum Electron. **30**, 249–264 (1998).
[208] M. V. D. Vermelho, U. Peschel, and J. S. Aitchison, J. Lightwave Technol. **18**, 401–408 (2000).
[209] C. Strohhöfer, and A. Polman, J. Appl. Phys. **90**, 4314–4320 (2001).
[210] A. D'Orazio, M. De Sario, L. Mescia, V. Petruzzelli, F. Prudenzano, A. Chiasera, M. Montagna, C. Tosello, and M. Ferrari, J. Non-Cryst. Solids **322**, 278–283 (2003).
[211] 3S Photonics, http://www.3sphotonics.com/.
[212] D. Bucci, J. Grelin, E. Ghibaudo, and J. E. Broquin, IEEE Photon. Technol. Lett. **19**, 698–700 (2007).
[213] L. H. Slooff, P. G. Kik, A. Tip, and A. Polman, J. Lightwave Technol. **19**, 1740–1744 (2001).
[214] S. Saini, C. Y. Hong, S. Bernardis, N. Pfaff, L. C. Kimerling, and J. Michel, Appl. Phys. Lett. **94**, 091117/1–3 (2009).
[215] F. Di Pasquale, S. Faralli, and V. Toccafondo, IEEE Photon. Technol. Lett. **19**, 1967–1969 (2007).
[216] V. Toccafondo, F. Di Pasquale, S. Faralli, N. Daldosso, L. Pavesi, and H. E. Hernandez-Figueroa, Opt. Express **15**, 14907–14913 (2007).
[217] V. Toccafondo, S. Faralli, and F. Di Pasquale, J. Lightwave Technol. **26**, 3584–3591 (2008).
[218] V. Donzella, S. Faralli, V. Toccafondo, and F. Di Pasquale, J. Lightwave Technol. **27**, 3342–3350 (2009).
[219] S. F. Li, C. L. Song, Q. J. Xiong, and B. Ran, Opt. Quantum Electron. **34**, 859–866 (2002).
[220] M. Federighi, and F. Di Pasquale, IEEE Photon. Technol. Lett. **7**, 303–305 (1995).
[221] Z. S. Xiao, R. Serna, C. N. Afonso, and I. Vickridge, Appl. Phys. Lett. **87**, 111103/1–3 (2005).
[222] C. Strohhöfer, and A. Polman, Appl. Phys. Lett. **81**, 1414–1416 (2002).
[223] M. K. Smit, G. A. Acket, and C. J. van der Laan, Thin Solid Films **138**, 171–181 (1986).
[224] K. Wörhoff, and M. Pollnau, Aluminum oxide thin films for optical applications, submitted (2011).
[225] W. B. Huang, and R. R. A. Syms, J. Lightwave Technol. **17**, 2658–2664 (1999).
[226] D. Lowe, R. R. A. Syms, and W. B. Huang, J. Lightwave Technol. **20**, 454–462 (2002).
[227] S. Saini, J. Michel, and L. C. Kimerling, J. Lightwave Technol. **21**, 2368–2376 (2003).
[228] D. Portch, R. R. A. Syms, and W. Huang, IEEE Photon. Technol. Lett. **16**, 1634–1636 (2004).

© 2011 by WILEY-VCH Verlag GmbH & Co. KGaA, Weinheim

[229] I. Mozjerin, S. Ruschin, and A. Hardy, Appl. Opt. **44**, 2659–2666 (2005).
[230] P. G. Kik, and A. Polman, J. Appl. Phys. **93**, 5008–5012 (2003).
[231] Y. Jaouën, L. du Mouza, D. Barbier, J.-M. Delavaux, and P. Bruno, IEEE Photon. Technol. Lett. **11**, 1105–1107 (1999).
[232] M. Ono, Y. Kondo, J. Kageyama, and N. Sugimoto, J. Ceram. Soc. Jpn. **116**, 1134–1138 (2008).
[233] K. Hattori, T. Kitagawa, and Y. Ohmori, J. Appl. Phys. **79**, 1238–1243 (1996).
[234] J. Shmulovich, Proc. SPIE **2996**, 143–153 (1997).
[235] Teem Photonics, http://www.teemphotonics.com/.
[236] CIP Technologies, http://www.ciphotonics.com/.
[237] K. C. Reichmann, P. P. Iannone, M. Birk, N. J. Frigo, D. Barbier, C. Cassagnettes, T. Garret, A. Verlucco, S. Perrier, and J. Philipsen, IEEE Photon. Technol. Lett. **13**, 1130–1132 (2001).
[238] K. Ennser, S. Taccheo, T. Rogowski, and J. Shmulovich, J. Lightwave, Technol. **25**, 1670–1675 (2007).
[239] K. Ennser, G. Della Valle, and S. Taccheo, J. Lightwave Technol. **27**, 88–93 (2009).
[240] J.-M. P. Delavaux, G. C. McIntosh, G. R. Wilson, J. Shmulovich, A. Kevorkian, and D. Barbier, Multiple carrier analog transmission system with Er^{3+} doped planar optical waveguide amplifiers, in: Conference on Optical Fiber Communication, Technical Digest Series, Baltimore, MD, 2000, paper FD3, pp. 1–3.
[241] C. M. McIntosh, J.-M. P. Delavaux, G. C. Wilson, C. Hullin, B. Neyret, J. Philipsen, C. Cassagnetes, and D. Barbier, High output power erbium doped waveguide amplifier for QAM distribution, in: Conference on Optical Fiber Communication, Technical Digest Series, Anaheim, CA, 2001, paper WDD5, pp. 1–3.
[242] K. Ennser, G. Della Valle, M. Ibsen, J. Shmulovich, and S. Taccheo, IEEE Photon. Technol. Lett. **17**, 1468–1470 (2005).
[243] K. H. Lai, and S. Chi, Jpn. J. Appl. Phys. Part 1 **44**, 4009–4011 (2005).
[244] S. Demiguel, N. Sahri, M. Hartlaub, F. Blache, H. Gariah, S. Vuiye, D. Carpentier, D. Barbier, and J. C. Campbell, Electron. Lett. **43**, 51–52 (2007).
[245] J. D. B. Bradley, M. C. E. Silva, M. Gay, L. Bramerie, A. Driessen, K. Wörhoff, J. C. Simon, and M. Pollnau, Opt. Express **17**, 22201–22208 (2009).
[246] M. W. Sckerl, S. Guldberg-Kjær, C. Laurent-Lund, and M. Rysholt Poulsen, Loss-less planar waveguide 1:4 power splitter at 1550 nm, in: Proceedings of the European Conference on Optical Communication, Nice, France, 1999, pp. 48–49.
[247] Z. He, Y. G. Li, Y. W. Zhang, D. X. Li, L. Y. Liu, and L. Xu, J. Korean Phys. Soc. **49**, 2159–2163 (2006).
[248] H. C. Chien, C. H. Yeh, and C. C. Lee, Opt. Eng. **44**, 044204/1–3 (2005).
[249] S. Y. Chou, C. H. Yeh, and S. Chi, Laser Phys. Lett. **4**, 382–384 (2007).
[250] C. H. Yeh, and S. Chi, Opt. Express **15**, 3680–3684 (2007).
[251] P. C. Peng, K. M. Feng, W. R. Peng, H. Y. Chiou, C. C. Chang, and S. Chi, Opt. Commun. **252**, 127–131 (2005).
[252] R. Brinkmann, M. Dinand, I. Baumann, C. Harizi, W. Sohler, and H. Suche, IEEE Photon. Technol. Lett. **6**, 519–521 (1994).
[253] H. Suche, D. Hiller, I. Baumann, and W. Sohler, IEEE Photon. Technol. Lett. **7**, 505–507 (1995).
[254] M. U. Staudt, S. R. Hastings-Simon, M. Nilsson, M. Afzelius, V. Scarani, R. Ricken, H. Suche, W. Sohler, W. Tittel, and N. Gisin, Phys. Rev. Lett. **98**, 113601/1–4 (2007).
[255] F. Di Pasquale, and H. E. Hernández-Figueroa, Electron. Lett. **30**, 232–233 (1994).
[256] C. Becker, T. Oesselke, J. Pandavenes, R. Ricken, K. Rochhausen, G. Schreiber, W. Sohler, H. Suche, R. Wessel, S. Balsamo, I. Montrosset, and D. Sciancalepore, IEEE J. Sel. Top. Quantum Electron. **6**, 101–113 (2000).
[257] M. Pollnau, and S. D. Jackson, IEEE J. Sel. Top. Quantum Electron. **7**, 30–40 (2001). Correction: IEEE J. Sel. Top. Quantum Electron. **8**, 956 (2002).
[258] R. Brede, T. Danger, E. Heumann, G. Huber, and B. H. T. Chai, Appl. Phys. Lett. **63**, 729–730 (1993).
[259] T. Kitagawa, F. Bilodeau, B. Malo, S. Thériault, J. Albert, D. C. Jihnson, K. O. Hill, K. Hattori, and Y. Hibino, Electron. Lett. **30**, 1311–1313 (1994).
[260] B. K. Das, H. Suche, and W. Sohler, Appl. Phys. B **73**, 439–442 (2001).
[261] H. S. Hsu, C. Cai, and A. M. Armani, Opt. Express **17**, 23265–23271 (2009).
[262] L. Yang, T. Carmon, B. Min, S. M. Spillane, and K. J. Vahala, Appl. Phys. Lett. **86**, 091114/1–3 (2005).
[263] B. K. Das, R. Ricken, V. Quiring, H. Suche, and W. Sohler, Opt. Lett. **29**, 165–167 (2004).
[264] D. L. Veasey, D. S. Funk, P. M. Peters, N. A. Sanford, G. E. Obarski, N. Fontaine, M. Young, A. P. Peskin, W. C. Liu, S. N. Houde-Walter, and J. S. Hayden, J. Non-Cryst. Solids **263**, 369–381 (2000).
[265] S. D. Conzone, J. S. Hayden, D. S. Funk, A. Roshko, and D. L. Veasey, Opt. Lett. **26**, 509–511 (2001).
[266] P. Becker, R. Brinkmann, M. Dinand, W. Sohler, and H. Suche, Appl. Phys. Lett. **61**, 1257–1259 (1992).
[267] J. D. B. Bradley, R. Stoffer, L. Agazzi, F. Ay, K. Wörhoff, and M. Pollnau, Opt. Lett. **35**, 73–75 (2010).
[268] W. Sohler, B. K. Das, D. Dey, S. Reza, H. Suche, and R. Ricken, IEICE Trans. Electron. **E88c**, 990–997 (2005).
[269] N. D. Psaila, R. R. Thomson, H. T. Bookey, N. Chiodo, S. Shen, R. Osellame, G. Cerullo, A. Jha, and A. K. Kar, IEEE Photon. Technol. Lett. **20**, 126–128 (2008).
[270] G. Jose, S. Taccheo, G. Sorbello, D. Migliorati, V. Foglietti, E. Cianci, S. Jiang, N. Peyghambarian, and P. Laporta, Electron. Lett. **38**, 1275–1276 (2002).
[271] G. Sorbello, S. Taccheo, G. Della Valle, P. Laporta, E. Cianci, V. Foglietti, S. Jiang, and N. Peyghambarian, Opt. Quantum Electron. **35**, 669–674 (2003).
[272] R. Osellame, N. Chiodo, G. Della Valle, G. Cerullo, R. Ramponi, P. Laporta, A. Killi, U. Morgner, and O. Svelto, IEEE J. Sel. Top. Quantum Electron. **12**, 277–285 (2006).
[273] A. Yeniay, J.-M. P. Delavaux, J. Toulouse, D. Barbier, T. A. Strasser, and J. R. Pedrazanni, IEEE Photon. Technol. Lett. **9**, 1099–1101 (1997).
[274] C. Becker, A. Greiner, T. Oesselke, A. Pape, W. Sohler, and H. Suche, Opt. Lett. **23**, 1194–1196 (1998).
[275] P. Madasamy, G. N. Conti, P. Poyhonen, Y. Hu, M. M. Morrell, D. F. Geraghty, S. Honkanen, and N. Peyghambarian, Opt. Eng. **41**, 1084–1086 (2002).
[276] S. Guldberg-Kjær, J. Hübner, M. Kristensen, C. Laurent-Lund, M. Rysholt Poulsen, and M. W. Sckerl, Electron. Lett. **35**, 302–303 (1999).

© 2011 by WILEY-VCH Verlag GmbH & Co. KGaA, Weinheim

[277] L. Bastard, S. Blaize, and J. E. Broquin, Opt. Eng. **42**, 2800–2804 (2003).
[278] G. D. Marshall, P. Dekker, M. Ams, J. A. Piper, and M. J. Withford, Opt. Lett. **33**, 956–958 (2008).
[279] K. Hattori, T. Kitagawa, M. Oguma, Y. Hibino, Y. Ohmori, and M. Horiguchi, Electron. Commun. Jpn. **77**, 62–72 (1994).
[280] J. Kalkman, A. Tchebotareva, A. Polman, T. J. Kippenberg, B. Min, and K. J. Vahala, J. Appl. Phys. **99**, 083103/1–9 (2006).
[281] H. Suche, R. Wessel, S. Westenhöfer, W. Sohler, S. Bosso, C. Carmannini, and R. Corsini, Opt. Lett. **20**, 596–598 (1995).
[282] H. Suche, A. Greiner, W. Qiu, R. Wessel, and W. Sohler, IEEE J. Quantum Electron. **33**, 1642–1646 (1997).
[283] S. Balsamo, S. Maio, I. Montrosset, H. Suche, and W. Sohler, Opt. Quantum Electron. **31**, 29–33 (1999).
[284] A. Yeniay, J. M. P. Delavaux, J. Toulouse, D. Barbier, T. A. Strasser, J. R. Pedrazanni, and W. Minford, IEEE Photon. Technol. Lett. **9**, 1580–1582 (1997).
[285] G. Della Valle, R. Osellame, G. Galzerano, N. Chiodo, G. Cerullo, P. Laporta, and O. Svelto, Appl. Phys. Lett. **89**, 231115/1–3 (2006).
[286] D. Pudo, H. Byun, J. Chen, J. Sickler, F. X. Kärtner, and E. P. Ippen, Opt. Express **16**, 19221–19231 (2008).
[287] H. Byun, D. Pudo, S. Frolov, A. Hanjani, J. Shmulovich, E. P. Ippen, and F. X. Kartner, IEEE Photon. Technol. Lett. **21**, 763–765 (2009).
[288] D. J. Jones, S. Namiki, D. Barbier, E. P. Ippen, and H. A. Haus, IEEE Photon. Technol. Lett. **10**, 666–668 (1998).
[289] J. Yang, and L. J. Guo, IEEE J. Sel. Top. Quantum Electron. **12**, 143–147 (2006).
[290] C. A. Barrios, and M. Lipson, Opt. Express **13**, 10092–10101 (2005).
[291] D. W. Prather, B. Redding, T. Creazzo, E. Marchena, and S. Shi, J. Nanosci. Nanotechnol. **10**, 1643–1649 (2010).
[292] L. Agazzi, J. D. B. Bradley, F. Ay, G. Roelkens, R. Baets, K. Wörhoff, and M. Pollnau, Opt. Express **18**, 27703–27711 (2011).

© 2011 by WILEY-VCH Verlag GmbH & Co. KGaA, Weinheim